

**1 Testing linearity and comparing linear response models
2 for global surface temperatures**

3 Hege-Beate Fredriksen^{1,2}, Kai-Uwe Eiselt¹and Peter Good³

4 ¹UiT the Arctic University of Norway, Tromsø, Norway

5 ²Norwegian Polar Institute, Tromsø, Norway

6 ³Met Office Hadley Centre, Exeter, United Kingdom

7 Key Points:

- 8** • We systematically compare different abrupt CO₂ change experiments from the Cou-
pled Model Intercomparison Project 6 and LongRunMIP archives
- 9** • Linear response is overall a good assumption, but there is some uncertainty in how
forcing varies with CO₂
- 10** • We derive a linear response model that can reproduce oscillations found in some
models, linked to ocean circulation and sea ice changes
- 11**
- 12**
- 13**

14 **Abstract**

15 Global temperature responses from different abrupt CO₂ change experiments participating
 16 in Coupled Model Intercomparison Project Phase 6 (CMIP6) and LongRunMIP are
 17 systematically compared in order to study the linearity of the responses. For CMIP6 mod-
 18 els, abrupt-4xCO₂ experiments warm on average 2.2 times more than abrupt-2xCO₂ ex-
 19 periments. A factor of about 2 can be attributed to the differences in forcing, and the
 20 rest is likely due to nonlinear responses. Abrupt-0p5xCO₂ responses are weaker than abrupt-
 21 2xCO₂, mostly because of weaker forcing. CMIP6 abrupt CO₂ change experiments re-
 22 spond linearly enough to well reconstruct responses to other experiments, such as 1pctCO₂,
 23 but uncertainties in the forcing can give uncertain responses. We derive also a generalised
 24 energy balance box model that includes the possibility of having oscillations in the global
 25 temperature responses. Oscillations are found in some models, and are connected to changes
 26 in ocean circulation and sea ice. Oscillating components connected to a cooling in the
 27 North Atlantic can counteract the long-term warming for decades or centuries and cause
 28 pauses in global temperature increase.

29 **Plain Language Summary**

30 We compare the global surface temperature responses in climate model experiments where
 31 the CO₂ concentration is abruptly changed from preindustrial levels and thereafter held
 32 constant. A quadrupling of CO₂ is expected to result in approximately twice the response
 33 to a doubling of CO₂. The ratio varies with time, but is on average 2.2 over the first 150
 34 years. A factor 2 can be attributed to the radiative forcing, that is, how much the en-
 35 ergy budget changes due to the change in CO₂. The remaining increase is likely due to
 36 stronger feedbacks. Experiments with half the CO₂ level are expected to have approx-
 37 imately the opposite response of a doubling, but we find their responses to be weaker.
 38 The reason appears to be a weaker radiative forcing. The evolution of the global tem-
 39 perature with time is also affected by changes in ocean heat uptake, ocean circulation,
 40 sea ice, cloud changes, etc., and these effects may be different with a stronger warming.
 41 Changes in the ocean circulation can also lead to oscillations appearing in addition to
 42 the warming. In some models, this effect may be strong enough to pause the long-term
 43 warming for decades or centuries, before it catches up again.

44 **1 Introduction**

45 Linear response is assumed for global surface temperature in many papers, resulting from
 46 e.g. box models (Geoffroy, Saint-Martin, Olivie, et al., 2013; Fredriksen & Rypdal, 2017;
 47 Caldeira & Myhrvold, 2013), and used in emulators like FaIR (Millar et al., 2017; Smith
 48 et al., 2018; Leach et al., 2021). It is based on the assumption that the global temper-
 49 ature response is independent of the climate state, and we can think of it as a power-
 50 ful first-order approximation of the temperature response to a perturbation of the top-
 51 of-atmosphere (TOA) energy budget. For strong enough responses, state-dependent mech-
 52 anisms like the albedo feedback will become important, so the question is: In what range
 53 of climate states can a linear response be considered a good assumption?

54 With a linear/impulse response model we can emulate the response to any known forc-
 55 ing within a few seconds, given knowledge about how the global temperature responds
 56 to an impulse. Alternatively, we can also gain this knowledge from step responses, since
 57 these are the integral of the impulse responses. The step-responses from experiments with
 58 abrupt quadrupling of the CO₂ concentration are typically used. This experiment is one
 59 of the DECK experiments required to participate in the Coupled Model Intercompar-
 60 ision Project (CMIP), and is therefore widely available.

61 Until recently, step-experiments with other CO₂ levels have only been available for a few
 62 models. Following the requests of nonlinMIP (Good et al., 2016), several CMIP6 mod-
 63 els now make abrupt-2xCO₂ and abrupt-0p5xCO₂ experiments available. In addition,

various abrupt CO₂ experiments are published through LongRunMIP (Rugenstein et al., 2019). The main motivation of this paper is to investigate the linearity of the temperature response by systematically comparing these different step experiments. That is, we want to test if the impulse response function derived from abrupt doubling of CO₂ experiments is equal (within expected uncertainties) to that derived from e.g. quadrupling of CO₂. This has implications for the concept of climate sensitivity – will the response to another doubling of CO₂ be similar to the first doubling?

In addition, we will discuss commonly used linear response models, derive the solution to a generalised box model, and study how well we can reconstruct the results of experiments that gradually increase the CO₂ concentration. With the generalised box model we demonstrate also how oscillations can appear in linear response models. The negative phase of oscillatory solutions may counteract the long-term warming for several decades, and these solutions can therefore be useful tools in understanding how plateaus or oscillations can appear in the global temperature responses to a step forcing, and how it is linked to changes in the ocean circulation and sea ice.

The generalised box model is described in Section 2. In Section 3 we discuss separation of forcing and response, and the linearity of global surface temperature response in the context of modifying the forcing-feedback framework to account for the non-constancy (or implicit time-dependence (Rohrschneider et al., 2019)) of global feedbacks. A non-constant feedback parameter just due to the pattern effect (a modulation of the global feedback from different paces of warming in different regions (Armour et al., 2013; Stevens et al., 2016; Andrews et al., 2015)) can be consistent with a linear response model, while state-dependent feedbacks imply a nonlinear response model. Section 4 describes the data included in this study and Section 5 describes estimation methods. Results are presented in sections 6 and 7, followed by a discussion in Section 8 and conclusions in Section 9.

2 Different linear response models, and their physical motivation

Generally, a linear response model for a climate state variable $\Phi(t)$ responding to a forcing $F(t)$ takes the form

$$\Phi(t) = G(t) * F(t) = \int_0^t G(t-s)F(s)ds, \quad (1)$$

assuming $F(t) = 0$ for $t \leq 0$ (Hasselmann et al., 1993). $G(t)$ is the Green's function, and $*$ denotes a convolution.

For global surface temperature, this integral can be interpreted as a part of the solution of a multibox energy balance model (see Fredriksen et al. (2021) and Appendix A),

$$\mathbf{C} \frac{d\mathbf{T}(t)}{dt} = \mathbf{K}\mathbf{T}(t) + \mathbf{F}(t) \quad (2)$$

where \mathbf{C} is a diagonal matrix of heat capacities of different components of the climate system, \mathbf{K} is a matrix of heat exchange coefficients, \mathbf{T} is a vector of temperature responses, and \mathbf{F} is a forcing vector. The two-box model (e.g. Geoffroy, Saint-Martin, Olivié, et al., 2013; Geoffroy, Saint-Martin, Bellon, et al., 2013; Held et al., 2010) is a widely used example. In appendix A we derive a general solution that can be applied to any linear K -box model, and find that in the case of only negative eigenvalues γ_n in the matrix $\mathbf{C}^{-1}\mathbf{K}$,

$$G(t) = \sum_{n=1}^K k_n e^{\gamma_n t}. \quad (3)$$

Hasselmann et al. (1993) notes that eigenvalues can also appear in complex pairs, where k_n and γ_n from one term of the pair are complex conjugates of the other term. To our knowledge, complex eigenvalues have never been used for estimating response functions in this field before. If pairs of complex eigenvalues are present, pairs from the sum above

96 can be replaced by damped oscillatory responses on the form $k_1 e^{pt} \cos qt + k_2 e^{pt} \sin qt$
 97 (see Appendix A). For these solutions to be stable, the real part of the eigenvalues (p)
 98 should be negative.

The step-forcing responses for negative eigenvalue solutions take the form:

$$T(t) = \sum_{n=1}^K S_n (1 - e^{\gamma_n t}) \quad (4)$$

and for complex eigenvalues, pairs from this sum are replaced by pairs on the form:

$$S_{osc1} \left[1 - e^{pt} \left(\cos qt - \frac{q}{p} \sin qt \right) \right] + S_{osc2} \left[1 - e^{pt} \left(\cos qt + \frac{p}{q} \sin qt \right) \right] \quad (5)$$

99 In these terms, the exponentially relaxing responses are modulated by sines and cosines.

100 So why do we want to expand the method to allow oscillatory responses for some mod-
 101 els? It is not given that all eigenvalues of the linear model have to be negative if we al-
 102 low the matrix \mathbf{K} to have asymmetric terms. Asymmetric terms could for instance ex-
 103 plain anomalies in energy fluxes following the ocean circulation, going only in one direc-
 104 tion between two boxes. So if for instance the Atlantic Meridional Overturning Circu-
 105 lation (AMOC) has a strong response, this might require complex eigenvalues in a lin-
 106 ear model for the surface temperature. And as we show in this paper, there are indeed
 107 models showing oscillations that can be described with such an oscillatory response func-
 108 tion.

109 Since there could be many configurations of the box model (with different physical in-
 110 terpretations) leading to the same solution, from now on we will just work with the pa-
 111 rameters in Eqs. (3, 4, 5) and not convert these to the parameters in the original box
 112 model in Eq. (2). When doing this we only have to specify the number of boxes used,
 113 and not worry about what is the best configuration of the boxes.

114 3 Distinguishing between forcing and response

The temperature response $T(t) = G(t) * F(t)$ cannot alone tell us how to distinguish
 between what is forcing and what is response to the forcing, since we can just move a
 factor between G and F without changing T . This separation is often done using the lin-
 ear forcing - feedback framework, expressing the global top-of-the-atmosphere radiation
 imbalance (N) as

$$N = F + \lambda T \quad (6)$$

115 where $\lambda < 0$ is the feedback parameter, T is the global temperature response and F
 116 is the radiative forcing. This tells us how we can use the additional knowledge about the
 117 time series N to distinguish between F and T . However, it is now well known that the
 118 feedback parameter is not well approximated by a constant, so several modifications to
 119 this framework have been proposed to account for this. Note that how N relates to T
 120 does not impact the mathematical structure of the temperature response (as long as it
 121 is a linear relation), only how the forcing and feedbacks should be defined.

122 We can distinguish between three main classes of modifications:

(1) Assuming that N is a nonlinear function of T , e.g:

$$N = F + c_1 T + c_2 T^2 \quad (7)$$

123 This describes how λ could change with state (temperature) (Bloch-Johnson et al., 2015,
 124 2021). Some examples of feedbacks that are well known to depend on temperature are
 125 the ice-albedo feedback and the water vapour feedback.

(2) Decomposing the surface temperature as

$$T = \sum_{n=1}^K T_n \quad (8)$$

and associate a feedback parameter λ_n with each component T_n , such that:

$$N = F + \sum_{n=1}^K \lambda_n T_n. \quad (9)$$

This can describe the pattern effect, if assuming different regions have different feedbacks and different amplitudes of the temperature response, which modulates the global value of λ with time (Armour et al., 2013). Proistosescu and Huybers (2017); Fredriksen et al. (2021, 2023) use such a decomposition of the temperature into linear responses with different time-scales.

Extending the decomposition of N in Eq. (9) to include oscillatory components may not be straight-forward if oscillations are in fact connected to the North Atlantic temperatures and changes in AMOC. The troposphere is very stable in this region and surface temperature changes are therefore confined in the lower troposphere, and not necessarily causing much change in the TOA radiation (Eiselt & Graversen, 2023; Jiang et al., 2023). Increasing surface temperatures in such stable regions lead to increased estimates of the climate sensitivity, interpreted as a positive lapse rate feedback (Lin et al., 2019). In the framework of Eq. (9) a possibility is to ignore or put less weight on the North Atlantic temperature component, due to the weaker connection between T and N here, but this needs to be further investigated in a future paper. Related effects can also play a role, for instance can AMOC changes lead to TOA radiation changes in surrounding areas, such as through low cloud changes in the tropics (Jiang et al., 2023). Such effects are likely model dependent.

(3) Descriptions using a heat-uptake efficacy factor ε , that describe how N depends on the heat uptake in the deeper ocean exist as well. This is mathematically equivalent to the second class for global quantities (Rohrschneider et al., 2019). In this description, the sum $T = \sum_{n=1}^K T_n$ is not necessarily considered a decomposition of the surface temperature, but includes also components describing temperature anomalies in the deeper ocean. If these temperatures are part of a linear model, typically a two- or three- box model, N can still be expressed as in Eq. (9). As these temperature components are just linear combinations of the components in Fredriksen et al. (2021); Proistosescu and Huybers (2017), it is only a matter of choice if expressing N using the temperatures in each box, or using the components of the diagonalized system, associated with different time scales of the system.

Descriptions with heat-uptake efficacy take slightly different forms in different papers. Winton et al. (2010) describes efficacy without specifying a model for the ocean heat uptake, while Held et al. (2010); Geoffroy, Saint-Martin, Bellon, et al. (2013) include it in the two-box model:

$$c_F \frac{dT}{dt} = -\beta T - \varepsilon H + F \quad (10)$$

$$c_D \frac{dT_D}{dt} = H \quad (11)$$

where T and T_D are the temperature anomalies of the surface and deep ocean boxes, respectively, and $H = \gamma(T - T_D)$ is the heat uptake of the deep ocean. The sum of the heat uptake in both layers equals N , leading to:

$$N = F - \beta T - (\varepsilon - 1)\gamma(T - T_D) \quad (12)$$

The concept of efficacy can be considered a way of retaining a "pattern effect" in box models with only one box connected to the surface, by relating the evolving spatial pattern of surface temperature change to the oceanic heat uptake (Held et al., 2010; Geoffroy & Saint-Martin, 2020). Similarly, efficacy of forcing (Hansen et al., 2005) has also been shown to be related to a "pattern effect" (Zhou et al., 2023), since forcing in different regions can trigger different atmospheric feedbacks.

Cummins et al. (2020); Leach et al. (2021) have modified this description to use it with a 3-box model, and use the heat uptake from the middle box to the deep ocean box to modify the radiative response

$$N(t) = F(t) - \lambda T_1(t) + (1 - \varepsilon) \kappa_3 [T_2(t) - T_3(t)] \quad (13)$$

If writing this equation in the form of Eq. (9), we find that the feedback parameters associated with $T_2(t)$ and $T_3(t)$ have equal magnitudes and opposite signs. This could put unfortunate constraints on parameters in this system, like net positive regional feedbacks, if interpreted as a pattern effect. We suggest avoiding this indirect description of the pattern effect with an efficacy parameter when using more than two boxes, and instead use a more direct interpretation of the parameters as describing a spatial pattern, such as Eq. (9).

3.1 Forcing defined using fixed-SST experiments

An alternative, that is not based on assumptions about the evolution of the feedbacks, is to run additional model experiments where sea-surface temperatures are kept fixed (Hansen et al., 2005; Pincus et al., 2016). These experiments aim to simulate close to 0 surface temperature change, such that $N \approx F$. Forcing estimated from these experiments have less uncertainty than regression methods based on the above-mentioned relationships between N , T and F (P. M. Forster et al., 2016), but are contaminated by land temperature responses. A forcing definition that includes all adjustments in N due to the forcing, but no adjustments due to surface temperature responses is the effective radiative forcing (ERF). This is considered the best predictor of surface temperatures, since it has forcing efficacy factors closest to 1 (Richardson et al., 2019). Ideally ERF should be estimated in models by fixing all surface temperatures, but this is technically challenging (Andrews et al., 2021). Instead, it is more common to correct the fixed-SST estimates for the land response (Richardson et al., 2019; Tang et al., 2019; Smith et al., 2020). We have not used these estimates in this paper, since they are not available for many models.

4 Choice of data

We compare abrupt-4xCO₂ global temperature responses to all other abrupt CO₂ experiments we can find. In the CMIP6 archive we have 12 models with abrupt-2xCO₂ and 9 models with abrupt-0p5xCO₂. In LongRunMIP we find 6 models with at least two different abrupt CO₂ experiments, and we use the notation abruptNx to describe these, where N could be 2, 4, 6, 8 or 16. The advantage of models in LongRunMIP is that we can study responses also on millennial time scales, while for CMIP6 models the experiments are typically 150 years long.

There exist also similar comparisons of abrupt CO₂ experiments for a few other models outside of these larger data archives (e.g., Mitevski et al., 2021, 2022; Meraner et al., 2013; Rohrschneider et al., 2019). These data are not analysed in this study, but will be included in our discussion.

CMIP6 abrupt CO₂ experiments are used to reconstruct 1pctCO₂ experiments, and the reconstructions are compared to the coupled model output of CMIP6 models. The reason for choosing this experiment is that the forcing is relatively well known. If assuming the forcing scales like the superlogarithmic formula of Etminan et al. (2016), it should increase slightly more than linearly until CO₂ is quadrupled, and end up at the same forc-

205 ing level as the abrupt-4xCO₂ experiments. The Etminan et al. (2016) forcing includes
 206 stratospheric adjustments, but not tropospheric and cloud adjustments like the ERF.
 207 However, we don't use the absolute values of this forcing, only the forcing ratios. We may
 208 also take these ratios as approximate ERF ratios if assuming the Etminan et al. (2016)
 209 forcing can be converted to ERF with a constant factor.

210 For other experiments, the uncertainty in forcing estimates is an even more important
 211 contribution to uncertainties in the responses. Jackson et al. (2022) test emulator responses
 212 to the Radiative Forcing Model Intercomparison Project (RFMIP) forcing for 8 mod-
 213 els, and find large model differences in emulator performance. Using a different forcing
 214 estimation method (Fredriksen et al., 2021) for the CMIP6 models, Fredriksen et al. (2023)
 215 find a generally good emulator performance for historical and SSP experiments. An im-
 216 portant difference between the forcing estimates is that the RFMIP forcing used by Jackson
 217 et al. (2022) is not corrected for land temperature responses, while the regression-based
 218 forcing in Fredriksen et al. (2023) is defined for no surface temperature response. The
 219 method described in Fredriksen et al. (2021, 2023) is actually designed to make forcing
 220 estimates compatible with a linear temperature response, and we therefore refer to these
 221 results for performance of linear response models for historical and future scenario forc-
 222 ing. However, if the linear response assumption is poor for the temperatures, this influ-
 223 ences performance of the forcing estimation method as well. For this reason it is impor-
 224 tant to test the linear response hypothesis with idealized experiments, which is the fo-
 225 cusing of this paper.

226 4.1 AMOC and sea ice

227 In our discussion of oscillatory responses and plateaus in global temperature, we con-
 228 sider also AMOC and sea ice changes in the models. The AMOC index is calculated as
 229 the maximum of the meridional overturning stream function (*mstfmz* or *mstfyz* in CMIP6
 230 and *moc* in LongRunMIP) north of 30°N in the Atlantic basin below 500 m depth.

231 The sea-ice area is calculated by multiplying the sea-ice concentration (*siconc* or *siconca*
 232 in CMIP6 and *sic* in LongRunMIP) with the cell area (*areacello* or *areacella*) and then
 233 summing separately over the northern and southern hemispheres.

234 5 Estimation

235 5.1 Forcing ratios for step experiments

236 A linear temperature response assumption predicts the response in any abrupt CO₂
 237 experiment to be a scaled version of that of the abrupt-2xCO₂ experiment, since only the
 238 forcing is different in these experiments. So when comparing abrupt CO₂ experiments,
 239 they are all scaled to correspond to the abrupt-2xCO₂ experiment. However, choosing
 240 the best scaling factor is challenging, since the forcing is uncertain, and it is not easy to
 241 distinguish between differences due to forcing and possible nonlinear temperature responses.
 242 Therefore, we have used three different types of scaling factors in our analysis:

- 243 1) Use the same scaling factor for all models, and assume a forcing scaling like the
 244 superlogarithmic radiative forcing (RF) formula in Etminan et al. (2016) in the
 245 CO₂ range where this formula is valid, and logarithmic forcing outside this range
 246 (just to have something in lack of a valid non-logarithmic description). The fac-
 247 tors used are 0.478 for abrupt-4xCO₂ and 0.363 for abrupt-6xCO₂. A logar-
 248 rhythmic dependence on the CO₂ concentrations results in the factors -1, 1/4 and 1/8
 249 for the abrupt- 0p5xCO₂, 8xCO₂ and 16xCO₂ experiments.
- 250 2) Estimate ratios by performing Gregory regressions (Gregory et al., 2004) of the
 251 first 5, 10, 20 and 30 years of the experiments.
- 252 3) Use the mean temperature ratio to the abrupt-2xCO₂ experiment over the first
 253 150 years as the scaling factor. This is not meant to be an unbiased estimate of
 254 the forcing ratio, but investigates the forcing ratios in the hypothetical case of per-

255 flectly linear responses. However, some degree of nonlinear response is expected
 256 e.g. from differences in feedbacks (Bloch-Johnson et al., 2021). After scaling tem-
 257 perature responses with this factor, it is easier to visualise how nonlinear responses
 258 affect different time scales of the response.

259 **5.2 Reconstructing 1pctCO₂ experiments**

Performing an integration by parts of Eq. (1) leads to

$$T(t) = \int_0^t \frac{dF}{ds} R(t-s) ds, \quad (14)$$

where $R(t) = \int_0^t G(t-s) ds$ is the response to a unit-step forcing. Discretising this equation leads to the expression used to compute impulse responses in Good et al. (2011, 2013, 2016); Larson and Portmann (2016):

$$T_i = \sum_{j=0}^i \frac{\Delta F_j R_{i-j}}{\Delta F_s} \quad (15)$$

260 where ΔF_j are annual forcing increments, and the discretised step response R_{i-j} is a re-
 261 sponse to a general step forcing ΔF_s , and must therefore be normalised with this forc-
 262 ing. Further details of the derivation are provided in Fredriksen et al. (2021) Supplemen-
 263 tary Text S2.

264 With Eq. (15) we can use datapoints from abrupt CO₂ experiments and knowledge of
 265 forcing to directly compute the responses to other experiments. Then we can avoid the
 266 additional uncertainty related to what model to fit and its parameter uncertainties. Fit-
 267 ting a box model first would smooth out internal variability from the step response func-
 268 tion, which could be an advantage when studying responses to experiments with more
 269 variable forcing. Another advantage of box models is that the response function can be
 270 extrapolated into the future, while with Eq. (15) the length of the reconstruction is re-
 271 stricted by the length of the step experiment. Here we will use 140 years of data for the
 272 reconstruction of 1pctCO₂ experiments, and as we will see, the reconstructed responses
 273 to 1pctCO₂ experiments are already very smooth, so smoothing the response function
 274 with exponential responses should not change the results significantly, as long as the smoothed
 275 model provides a good fit to the datapoints.

276 To test this reconstruction, we will use CMIP6 annual anomalies from the experiments
 277 abrupt-4xCO₂, abrupt-2xCO₂ and abrupt-0p5xCO₂. The input forcing ratio starts at
 278 0, and increases either linearly, consistent with a logarithmic dependence on CO₂ con-
 279 centration, or as a ratio scaling like the superlogarithmic formula (Etminan et al., 2016).
 280 For abrupt-4xCO₂, we assume the ratio becomes 1 in year 140, the time of quadrupling,
 281 and for abrupt-2xCO₂, we assume the ratio is 1 in year 70, the time of doubling. The
 282 positive 1pctCO₂ forcing does not equal the negative abrupt-0p5xCO₂ forcing at any
 283 time point, so we just assume the abrupt-0p5xCO₂ forcing to be the negative of the abrupt-
 284 2xCO₂ forcing.

285 **5.3 Fitting response functions**

286 We will compare estimated response models from a two-box model, three-box model, and
 287 a four-box model with one pair of complex eigenvalues. These response models consist
 288 of two or three exponential responses, or two exponential plus two damped oscillatory
 289 responses. Decomposing the response using box models may also help us gain insight into
 290 the physical reasons why a linear response model works or not.

291 We apply the python package lmfit to estimate the parameters of the response models.
 292 It takes in an initial parameter guess, and then searches for a solution that minimizes
 293 the least-squared errors. The final parameter estimates can be sensitive to the initial guesses,

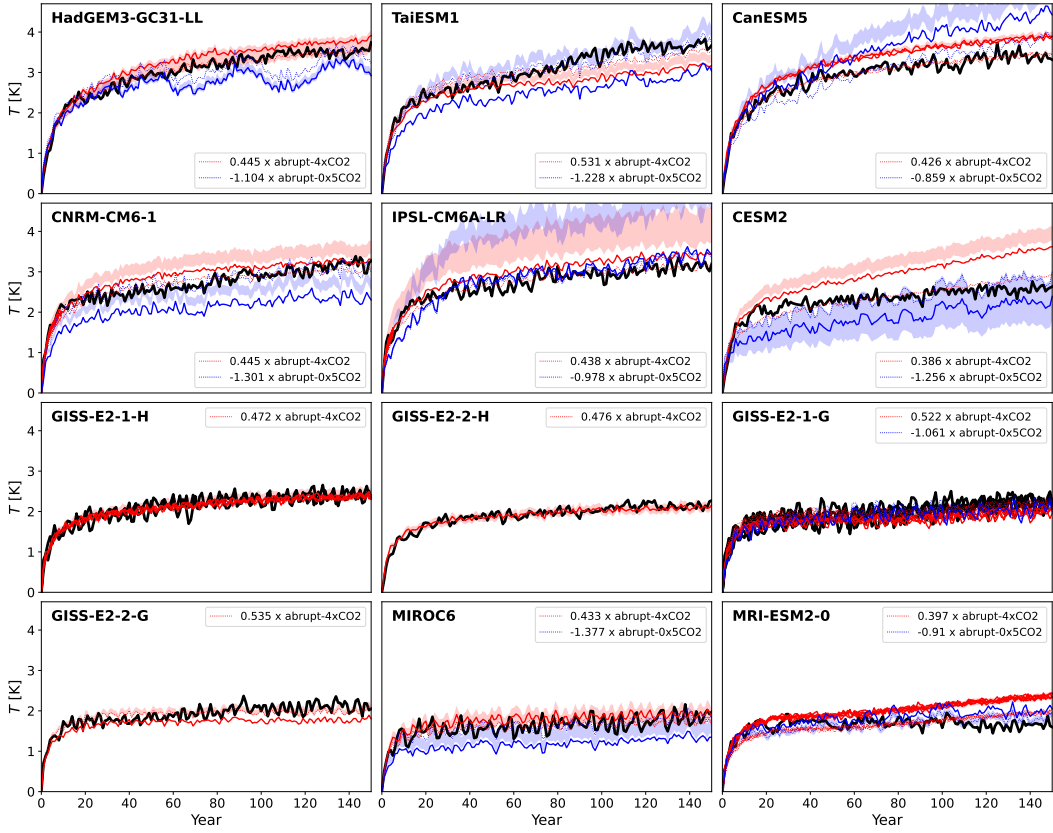


Figure 1. Comparing abrupt CO₂ experiments for CMIP6 models, where the abrupt-4xCO₂ and abrupt-0p5xCO₂ experiments are scaled in three different ways to correspond to the abrupt-2xCO₂ experiment. Models are sorted by their abrupt-2xCO₂ response in year 150. The black curves are abrupt-2xCO₂ experiments, the red are scaled abrupt-4xCO₂ and the blue are scaled abrupt-0p5xCO₂ experiments. Solid curves use the same scaling factor for all models: 0.478 for abrupt-4xCO₂ and -1 for abrupt-0p5xCO₂. Thin dotted curves use the mean temperature ratio as the scaling factor (shown in legends and supplementary figure S1), and shading shows the range of the ratios of the Gregory regressions given in Supporting Tables S1 and S2.

since the optimization algorithm may just have found a local minimum. The more parameters we have in the model, the less we can trust the estimates. We see this in particular when including oscillatory responses; then we need to estimate 8 parameters, and are at risk of overfitting for the typical 150 year long experiments. As we will see, there could be different solutions containing oscillations that all provide good fits to the data. Longer time series (or some physical reasoning) would be needed in order to select the optimal fit for these records. For longer time series such as those from LongRunMIP we obtain more useful estimates.

6 Linear response results

6.1 Comparing abrupt CO₂ experiments

The curves in Figures 1 and 2 are all scaled to correspond to the abrupt-2xCO₂ experiment, where the different scaling factors used illustrate the problem with the forcing uncertainty. The thick solid curves use the same scaling factor for all models (method 1), while the factors from the second and third method are model specific. The shading shows the range using the four different forcing ratios computed with Gregory regressions (method

2), that is, the minimum and maximum values from Tables S1 - S3. The thin dashed curves use the mean temperature ratios (method 3). These values are given in the subfigure legends, and shown in supporting figures S1 - S2. By definition, the black curves and the dotted red and blue curves all have the same time mean. Model specific factors can be explained by their different fast adjustments to the instantaneous radiative forcing. In addition, models can have different instantaneous forcing values, as this is shown to depend on the climatological base state (He et al., 2023). From the mean temperature ratios of the first 150 years of CMIP6 we find also that abrupt-4xCO₂ warms on average 2.2 times more than abrupt-2xCO₂, and abrupt-0p5xCO₂ cools on average 9 % less than abrupt-2xCO₂ warms (see Table S4). For LongRunMIP, abrupt4x warms 2.13 times abrupt2x when averaging all available years, or 2.18 times if averaging just the first 150 years (see Table S5, and both estimates exclude FAMOUS).

Significant differences between the curves in Figures 1 and 2 that cannot be explained by their different forcing must be explained by a nonlinear/state-dependent response. A first order assumption could be that models that warm more should tend to be more nonlinear. To investigate this we have ordered the models by their abrupt-2xCO₂ response in year 150 in Figure 1 and year 500 for the longer experiments in Figure 2. We find that there are some clear differences for the warmest CMIP6 models, but also for the coldest (MRI-ESM2-0). The four different GISS models appear to be very linear.

For the two LongRunMIP models with the strongest 2xCO₂ warming (CNRM-CM6-1 and FAMOUS) there are some clear differences between the curves (see Figure 2). The initial warming for CNRM-CM6-1 is halted in the 2xCO₂ compared to the 4xCO₂ experiment. For FAMOUS the scaling factor is particularly uncertain, and after a few centuries the pace of warming is slower in the scaled abrupt-4xCO₂ experiment than in the abrupt-2xCO₂ experiment. We observe only minor differences for MPI-ESM1-2, HadCM3L and CCSM3 when scaling with the mean temperature ratios. For CESM104 we observe that the abrupt2x experiment has some oscillations that are not seen in the other experiments, in addition to an abrupt change in the abrupt8x experiment.

If more warming increases the likelihood of finding nonlinear responses, we should also expect nonlinear responses to become more apparent towards the end of the simulations. We can then hypothesize that differences in forcing should explain initial differences (maybe up to a decade), and nonlinear responses explain differences at later stages. Following this, we should put more trust in the forcing scaling factors that make the initial temperature increase most similar to the abrupt-2xCO₂ experiment. Which factor this is differs between models. In general, method 2 should put more emphasis on describing the first years correctly, while method 3 emphasises a good fit on all scales.

Although the individual forcing estimates are uncertain, it is a noteworthy result that the abrupt-2xCO₂ regression forcing (method 2) is on average half of the abrupt-4xCO₂ forcing (see Tables S1 and S3). The uncertainty of this mean is however too large to rule out that the forcing for a second CO₂ doubling is in fact larger than the first doubling, according to the findings of Etminan et al. (2016); He et al. (2023). And consistent with these expectations, for CMIP6 abrupt-0p5xCO₂ we find a weaker negative forcing than logarithmic (Table S2). Our forcing ratios based on the LongRunMIP simulations for abrupt 6x, 8x and 16x CO₂ indicate that the forcing is weaker than logarithmic for higher CO₂ concentrations. Although based on very few simulations, this result is the opposite of the expectation that each CO₂ doubling produces stronger forcing (He et al., 2023).

An average forcing factor of 2 means the forcing alone is unlikely to explain the 2.2 factor difference in warming between CMIP6 abrupt-2xCO₂ and abrupt-4xCO₂. This conclusion is also supported by the differences in the pace of warming between abrupt-2xCO₂ and abrupt-4xCO₂ for several models (best visualised with the dotted curves from method 3 in Figure 1). The abrupt-4xCO₂ temperatures scaled using method 2 in Figure 1 are

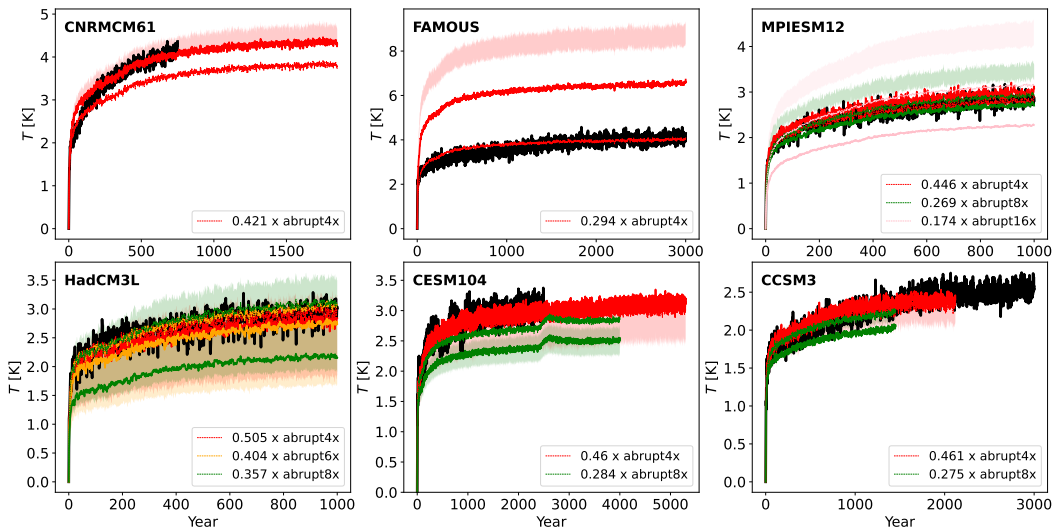


Figure 2. Comparing abrupt CO₂ experiments for LongRunMIP models. The scaling factors for the thick curves are 0.478 for 4x, 0.363 for 6x, 1/4 for 8x, 1/8 for 16x. For the thin dashed curves, the factors are computed from the mean T ratios to the first 150 years of abrupt2x, shown in Supporting figure S2, and shown in the legends here. The models are sorted by their abrupt2x temperature response in year 500. Note their different lengths and temperature scales.

on average 10 % stronger than the abrupt-2xCO₂ experiments (computed from the ratio 2.2/2). The scaled abrupt-0p5xCO₂ temperatures are on average 2 % stronger than the abrupt-2xCO₂ temperatures (see Table S4), suggesting that the weak forcing can explain much of the weak response for abrupt-0p5xCO₂. For LongRunMIP models, the average forcing ratio between 2x and 4x CO₂ reduces to 0.46 when excluding FAMOUS, making differences in the scaled temperatures over the first 150 years vanish (computed with method 2, see Table S5). For some models (CESM104 and CCSM3) the scaled temperatures deviate more from abrupt2x on millennial time scales.

Bloch-Johnson et al. (2021) suggests that feedback temperature dependence is the main reason why abrupt-4xCO₂ warms more than twice the abrupt-2xCO₂. This is consistent with the nonlinear responses we observe for several models. If the mean temperature ratio was a valid estimate of the forcing ratio, then in a linear framework, the same factors we found for the temperature ratios should be able to explain the ratios in top-of-atmosphere radiative imbalance. For some models this is not a good approximation (see supporting figures S1 and S2), consistent with the findings of Bloch-Johnson et al. (2021). FAMOUS has a particularly large difference in T and N ratios. Its abrupt4x warming is also so extreme that the quadratic model in Bloch-Johnson et al. (2021) suggests a runaway greenhouse effect.

378 **6.2 Reconstructing 1pctCO₂ experiments**

379 In general, we find that both abrupt-4xCO₂ experiments (see Figure 3) and abrupt-2xCO₂
 380 experiments (see Figure 4) can reconstruct the 1pctCO₂ experiment very well. The largest
 381 deviation we find for the model KIOST-ESM, but we suspect the 1pctCO₂ experiment
 382 from this model may have errors in the branch time information or the model setup. For
 383 many models the abrupt-0p5xCO₂ experiment can also be used to make a good recon-
 384 struction, but not all (see Figure 4). For several models where abrupt-0p5xCO₂ makes
 385 a poor reconstruction (TaiESM1, CNRM-CM6-1, CESM2, MIROC6), our assumptions
 386 about the forcing seems to be the limiting factor. If upscaling the negative of the abrupt-
 387 0p5xCO₂ response for these models with a different factor than -1 to correspond bet-
 388 ter with the abrupt-2xCO₂ experiment, we would have obtained a better reconstruction
 389 of 1pctCO₂.

390 For many models we find that reconstructions with abrupt-4xCO₂ slightly overestimates
 391 the 1pctCO₂ response in the middle parts of the experiment, similar to earlier findings
 392 by Good et al. (2013); Gregory et al. (2015). In Figure 3 we compare reconstructions with
 393 a linear forcing (from logarithmic dependence on CO₂) and a forcing scaling like the su-
 394 perlogarithmic formula (Etminan et al., 2016). We find that reconstructions using the
 395 superlogarithmic forcing (shown in brown) explains the middle part of the 1pctCO₂ ex-
 396 periment a little better than the logarithmic forcing (shown in red), since this forcing
 397 is slightly weaker in the middle. Even with the superlogarithmic forcing ratio, the model
 398 average reconstruction with abrupt-4xCO₂ is a little overestimated in the middle part
 399 of the experiment (Figure 5). The average reconstruction with abrupt-2xCO₂ explains
 400 the middle part of the experiment well, but slightly underestimates the latter part.

401 Which of abrupt-2xCO₂ or abrupt-4xCO₂ make the best reconstruction is model depen-
 402 dent. The 1pctCO₂ experiment goes gradually to 4xCO₂, and if there is a state-dependence
 403 involved in the response, we might expect something in between abrupt-2xCO₂ and abrupt-
 404 4xCO₂ responses to make the best prediction. MRI-ESM2-0 is a good example where
 405 this might be the case. For this model we observe a small underestimation with abrupt-
 406 2xCO₂ and a small overestimation with abrupt-4xCO₂. The reconstruction is very good
 407 with abrupt-0p5xCO₂, which has an absolute response looking like an average of abrupt-
 408 2xCO₂ and abrupt-4xCO₂ (see Figure 1). CESM2 is also a good example where state-
 409 dependent effects are visible, since the abrupt-2xCO₂ underestimates and abrupt-4xCO₂
 410 overestimates the response in the latest decades of the 1pctCO₂ experiment.

411 For TaiESM1 and CNRM-CM6-1 the paces of warming differ a little for abrupt-2xCO₂
 412 and abrupt-4xCO₂ during the middle/late stages of the experiments. Although the dif-
 413 ferences are not very significant, this is an indication of a nonlinear response. For some
 414 models (CanESM5, CNRM-CM6-1, HadGEM3-GC31-LL, IPSL-CM6A-LR, MIROC6)
 415 it is unclear if the small errors in the reconstructions are due to incorrect scaling of the
 416 forcing or nonlinear responses. The four GISS models are the most linear models, where
 417 we make good and very similar reconstructions with both abrupt-4xCO₂ and abrupt-
 418 2xCO₂. We observe just a small underestimation in the end of the experiment for GISS-
 419 E2-2-G abrupt-4xCO₂.

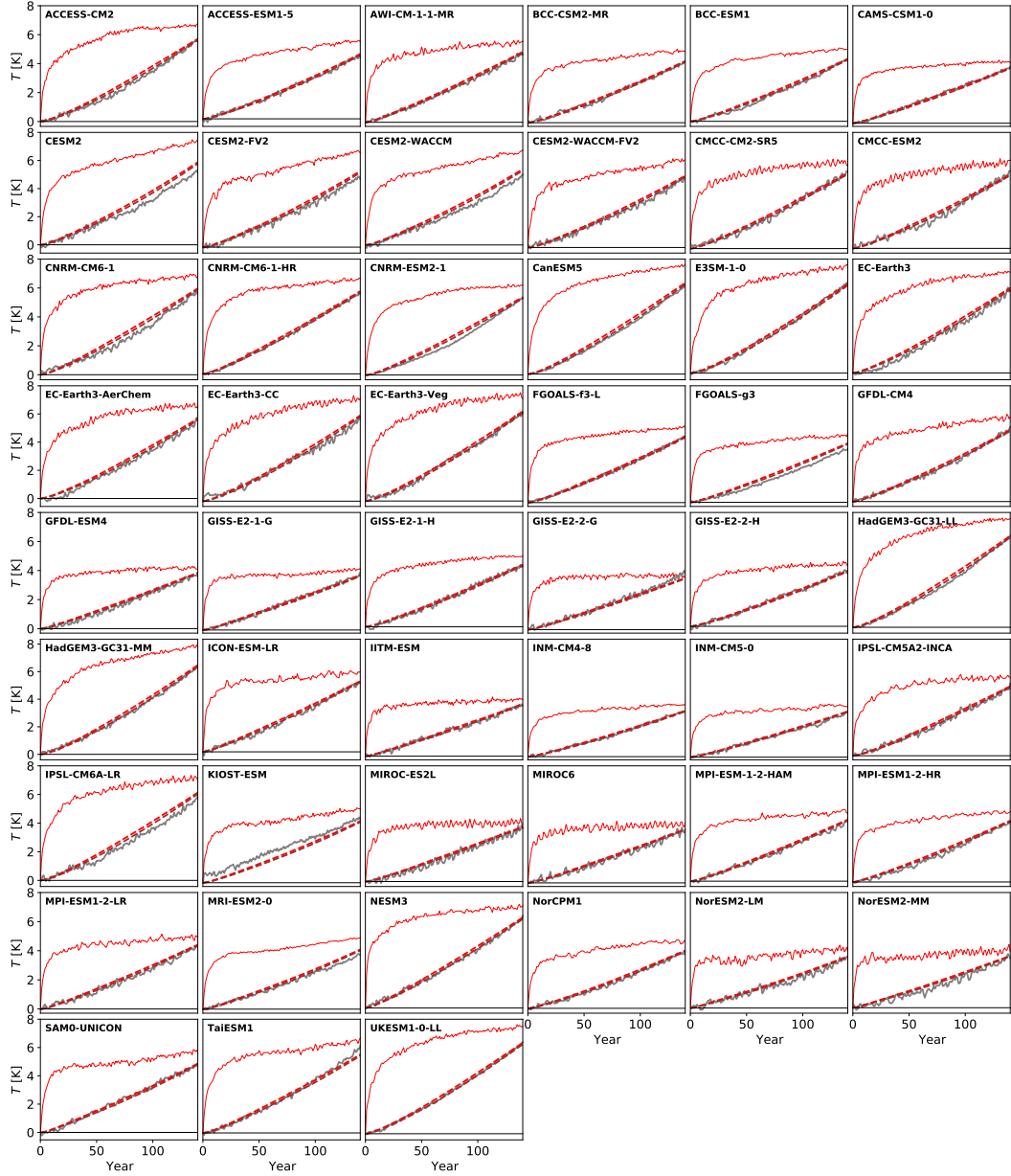


Figure 3. Red/brown dashed curves show reconstructions of the 1pctCO₂ experiment (gray) using the data from the abrupt-4xCO₂ experiment (red). The dashed red curve is a reconstruction based on a linearly increasing forcing, and the dashed brown curve is a reconstruction based on a forcing scaling like the superlogarithmic (Etminan et al., 2016) formula. For the experiments where several members exist, we have plotted the ensemble mean.

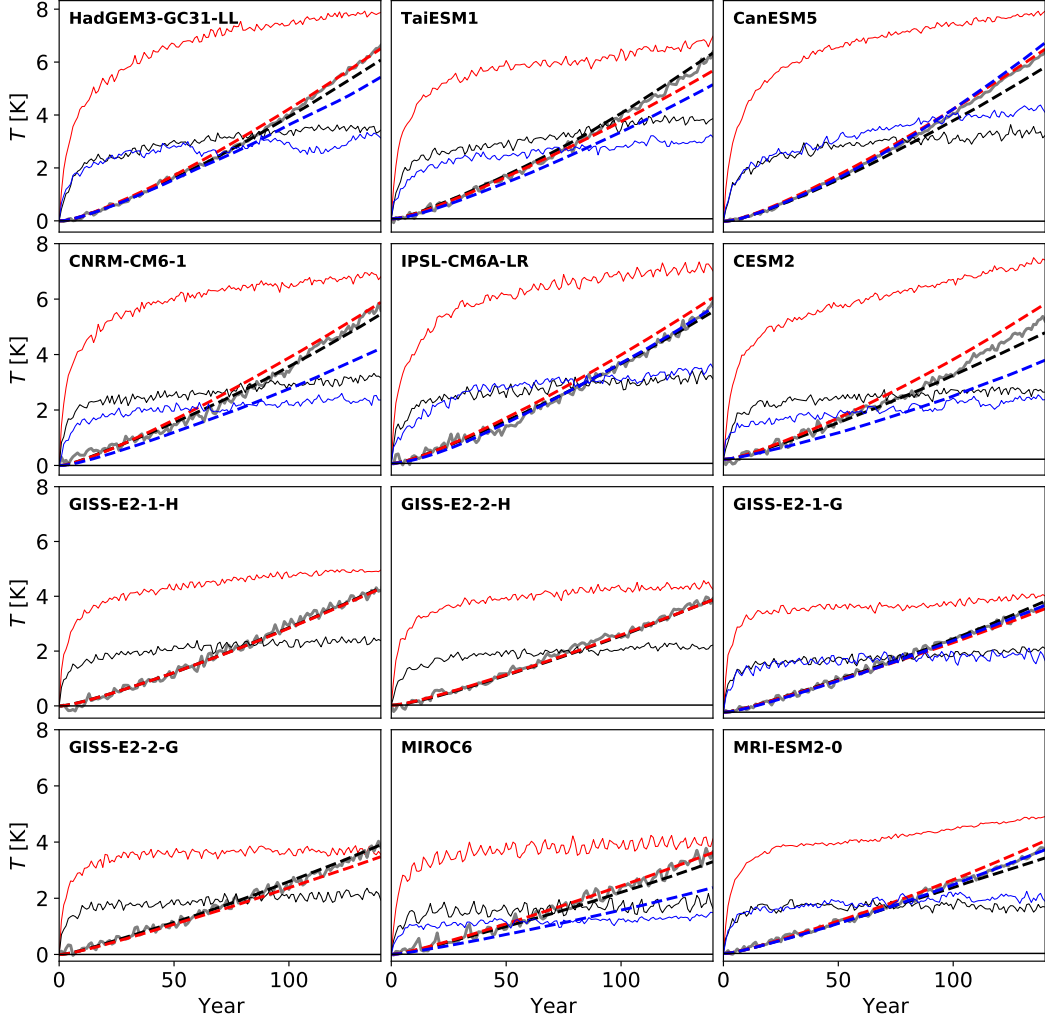


Figure 4. The dashed curves are reconstructions of the 1pctCO₂ experiment (gray) using data from the abrupt-4xCO₂ (red), abrupt-2xCO₂ (black) and abrupt-0p5xCO₂ (blue) experiments (solid curves). The forcing is assumed to scale like the superlogarithmic forcing in the reconstruction. The sign is flipped when plotting data from the abrupt-0p5xCO₂ experiment. For the experiments where several members exist, we have plotted the ensemble mean.

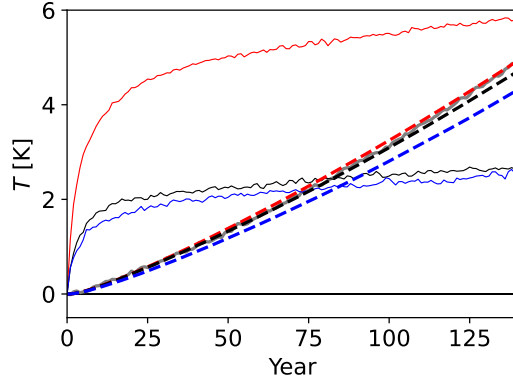


Figure 5. The model means of all curves in Figure 4.

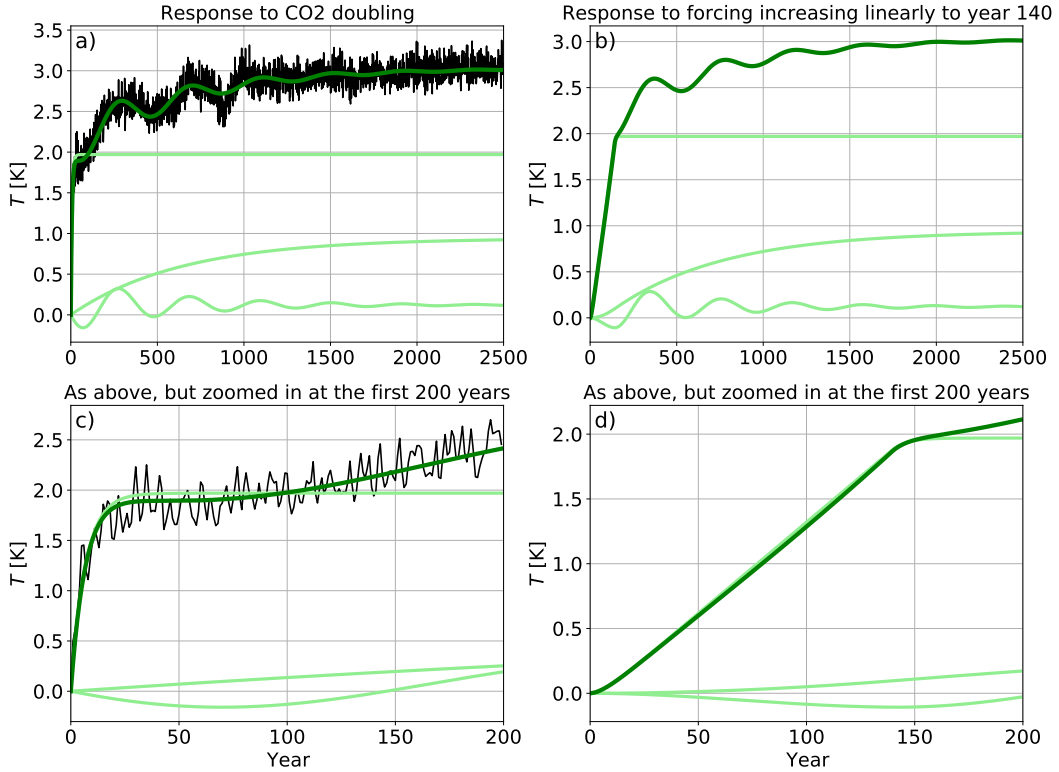


Figure 6. a) Result of fitting a two-exp and a pair of oscillatory responses to CESM104 abrupt2x. The dark green curves are the total responses to either an abrupt doubling of CO₂ (left) or a forcing increasing linearly to doubling of CO₂ in year 140, and is thereafter kept constant (right). The light green curves are components of the total response: Two exponential responses with time scales of approximately 7 and 639 years, and one oscillatory response with a period of approximately 410 years and damping time scale of 619 years.

6.3 Comparing different response functions

We fit two-exp, three-exp and two-exp + oscillatory response for all CMIP6 models. The resulting root mean squared error (RMSE) of these fits are summarised in Tables S6 and S7 for abrupt-4xCO₂, Table S8 for abrupt-2xCO₂ and Table S9 for abrupt-0p5xCO₂. The results for LongRunMIP experiments are listed in Table S10. As expected, RMSE is always smaller or unchanged for the three-exp model compared to the two-exp model. With an ideal estimation method, the two-exp + osc. should be reduced to a three-exp (by setting $q = 0$ and $S_2 = 0$) if the oscillatory solution is not a better description than the three-exp. Hence all results here with increased RMSE are just the results of not finding the optimal parameters. However, for the models where we estimate higher RMSE values for the two-exp + osc, this model is very unlikely to be a good description. Going further, we will therefore just focus on the models where adding oscillations provides a better description.

Including oscillations provides a smaller RMSE compared to the three-exp model for 11/22 LongRunMIP abrupt experiments. For most of these experiments, the improvement is very minor, and probably not worth the additional parameters. However, for one of these simulations an oscillatory response provides a visually significant better description: the CESM104 abrupt2x, shown in Figure 6 a). This experiment is also studied in further detail in Section 7.1 and Figure 8.

439 In Figure 6 b) and d) we estimate the temperature response to a forcing that increases
 440 linearly until doubling (in year 140), and is then kept constant thereafter. This will be
 441 approximately half the output of 1pctCO₂ experiments, and demonstrates that with this
 442 linear oscillatory model, the oscillations cannot be seen during the 140 years with lin-
 443 ear forcing. The negative response of the oscillatory part is to a large degree cancelled
 444 out by the slow exponential part, and the majority of the temperature response is de-
 445 scribed by the fastest exponential response.

446 42/71 runs for CMIP6 abrupt-4xCO₂ have smaller RMSE if including oscillations (note
 447 that we count different members from the same model). Also for these models, most im-
 448 provements are so minor that we cannot really argue that the extra parameters are needed.
 449 Despite large estimation uncertainties for these shorter runs, we find indications that there
 450 may be oscillations in many models. In the following, we highlight results for members
 451 from the 8 models where we have the largest improvements in RMSE for abrupt-4xCO₂:
 452 ACCESS-CM2, GISS-E2-1-G, ICON-ESM-LR, KIOST-ESM, MRI-ESM2-0, NorESM2-
 453 LM, SAM0-UNICON, TaiESM1. We note the generally close resemblance between these
 454 runs (see Figure 7) and the first 150 years of the CESM104 abrupt2x run in Figure 6 c).

455 The two-exp and oscillatory fits in Figure 7 show that the oscillatory component can take
 456 various shapes. For most members (e.g. TaiESM1 r1i1p1f1), the best fit includes an os-
 457 cillatory component that resembles the purely exponential components, but where the
 458 initial warming overshoots before stabilizing at a lower equilibrium temperature. In these
 459 cases the estimated oscillations have a quick damping time scale (τ_p), typically 20–30 years.
 460 For MRI-ESM2-0 members r7 and r10 we have instead an oscillation starting with an
 461 initial cooling, which is part of a slow oscillation that could develop as in the CESM104
 462 abrupt2x run. When including this slow oscillation, we find only shorter time scales (an-
 463 nual and decadal) for the two purely exponential parts. For the members where the os-
 464 cillation has a shorter period, we have a centennial-scale purely exponential part to ex-
 465 plain the slow variations in the temperature. Since we know from longer runs that a centennial-
 466 millennial scale exponential component is necessary to explain the full path to equilib-
 467 rium, the fits for MRI-ESM2-0 members r7 and r10 are unlikely to explain the future
 468 of these experiments. This could in theory be resolved by combining the two short time-
 469 scale exponential parts to one, and allowing the second exponential part to take a long
 470 time scale instead. However, with only 150 years of data, a fit containing several com-
 471 ponents varying on centennial to millennial scales will be poorly constrained. The take-
 472 home message from this is that we cannot really tell from the global surface tempera-
 473 ture of these short experiments if we deal with a short-period and quickly damped out
 474 oscillation or an oscillation lasting for centuries. Longer experiments are needed, but a
 475 closer look at the AMOC evolution and the spatial pattern of warming may also give some
 476 hints.

477 Of these 8 models, 3 models have also run abrupt-2xCO₂ and abrupt-0p5xCO₂ exper-
 478 iments. We see no clear signs of oscillations in these abrupt-0p5xCO₂ runs. For GISS-
 479 E2-1-G abrupt-2xCO₂ we observe a small flattening out of the temperature as for abrupt-
 480 4xCO₂, for MRI-ESM2-0 abrupt-2xCO₂ the temperature flattens out, and does not start
 481 to increase again. For TaiESM1 abrupt-2xCO₂, the temperature behaves similarly as for
 482 abrupt-4xCO₂ (although our estimated decomposition looks a bit different). Hence there
 483 are hints that the same phenomenon appears also for abrupt-2xCO₂, but the responses
 484 may not be perfectly linear.

485 7 Oscillations and plateaus in global temperatures

486 7.1 Oscillation in CESM1 warming experiments

487 The CESM1 abrupt CO₂ responses are further investigated (Figure 8) by looking at the
 488 Northern Hemisphere (NH) and Southern Hemisphere (SH) temperatures separately (a),
 489 and by comparing with the AMOC index (b) and NH and SH sea ice areas (c). We find
 490 that the oscillations happen only in the NH, and that the abrupt2x (blue) NH temper-

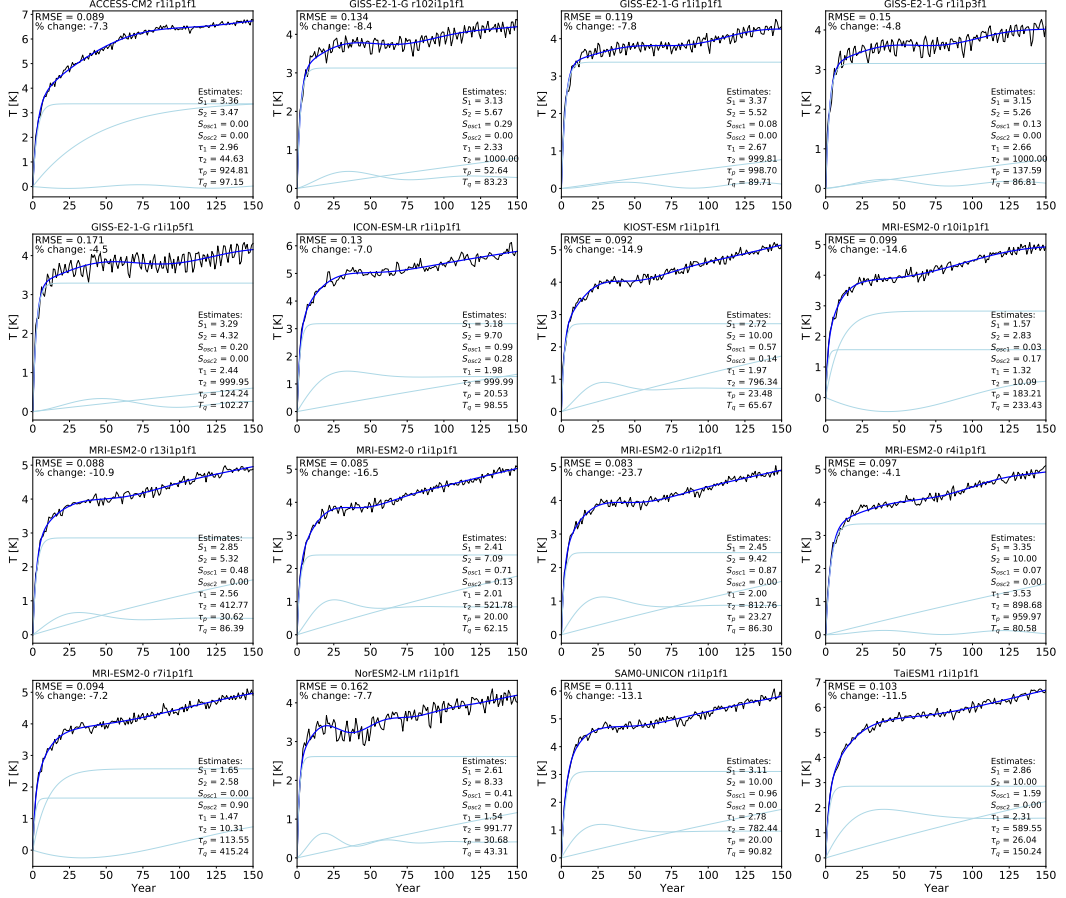


Figure 7. The two-exponential + oscillatory model fits (blue curves) for 16 different abrupt-4xCO₂ runs (black curves). The light blue curves show the decomposition of the blue curve into two exponential components and one oscillatory component. The estimated parameters are listed in the figures, and the % change refers to the improvement in RMSE from three-exponential fit to the two-exponential + oscillatory model fit.

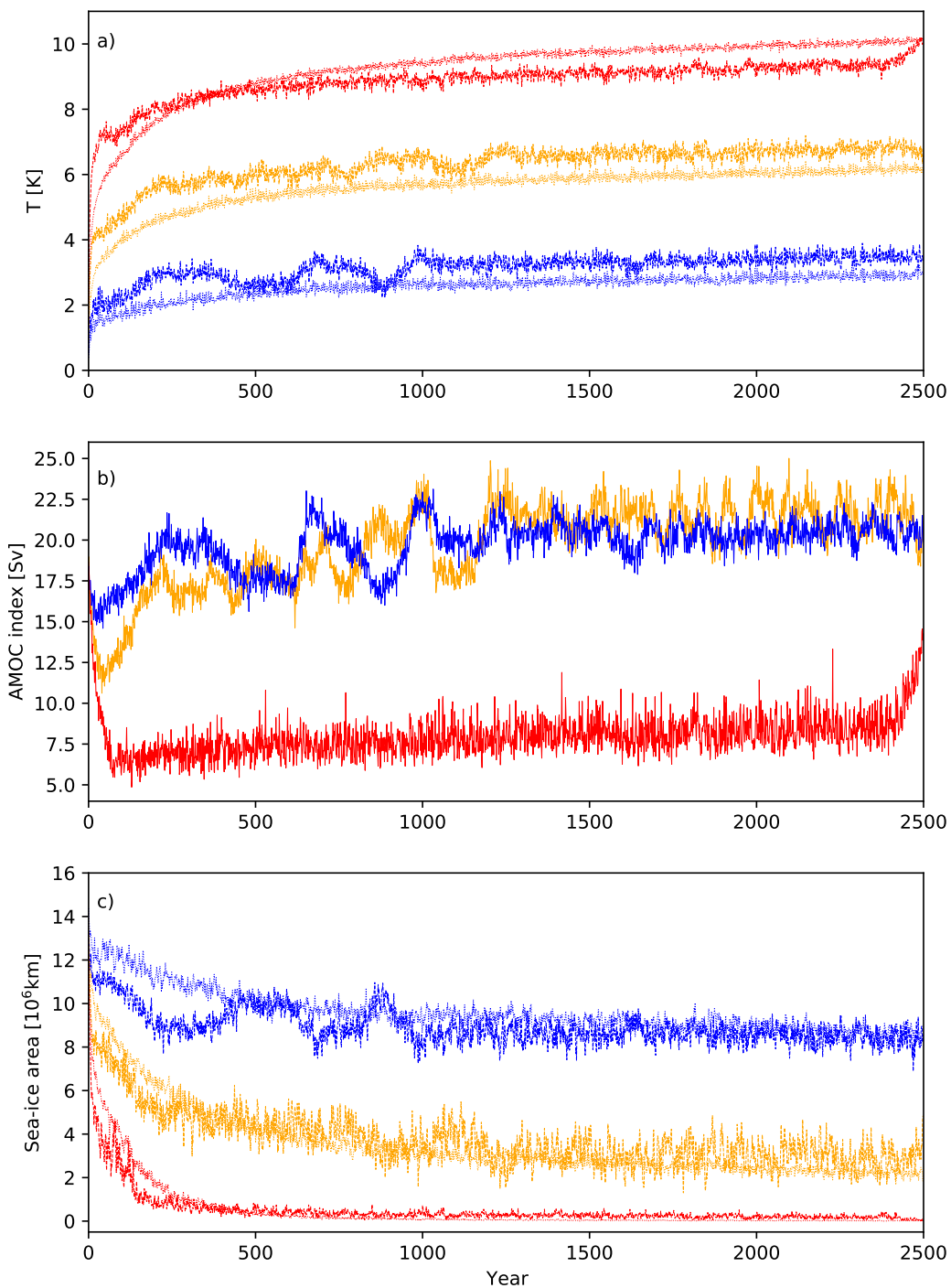


Figure 8. Mean surface temperature (a), AMOC index (b) and sea-ice area (c) for CESM104 abrupt2x (blue), abrupt4x (orange) and abrupt 8x (red). In a) and c), dashed curves are means over the Northern Hemisphere, and dotted (thinner) curves are means over the Southern Hemisphere.

ature is strongly correlated with the AMOC index ($R = 0.796$) and anticorrelated with the NH sea ice area ($R = -0.919$) if using all 2500 annual values for computation. If looking only at the first decades after the abrupt CO₂ doubling, we observe an anticorrelation between temperatures (which increase) and AMOC (which weakens). A plausible mechanism for this is that the strong initial warming inhibits the sinking of water in the North Atlantic by reducing its density. On longer time scales, AMOC changes also impact temperatures, by bringing more/less warm water northwards, which could explain the positive correlation.

The comparison with the abrupt 4x (orange) and 8x (red) simulations from the same model shows that all NH temperatures have a small plateau for some decades after the initial temperature increase, likely connected to their initial decrease in AMOC strength and sea-ice area. There are also some long-term variations later on in these experiments, but not following a similar oscillatory behaviour as the 2x experiment. We note for instance that the abrupt change around year 2500 in the abrupt8x experiment is strongly connected to an AMOC recovery. Hence, while linear response models estimated from the abrupt2x simulation may well describe the long-term responses to these other abrupt CO₂ experiments, the oscillatory behavior does not transfer to the same degree. In lack of more simulations with weaker forcing from this model, it is difficult to judge if the oscillatory phenomenon really is part of a linear model that can only be used for weaker forcings, or if it is a nonlinear effect or a random fluctuation.

511 7.2 Oscillation in cooling HadGEM experiment

512 Among models with abrupt-0p5xCO₂ experiments, we find one (HadGEM-GC31-LL)
 513 with an interesting oscillation. This oscillation appears to have an increasing amplitude
 514 (see Figure 9 a)). To fit our model to these data, we need to allow the oscillatory part
 515 of the solution to have a positive real part eigenvalue, such that we get unstable/growing
 516 oscillations. This corresponds to a negative damping time scale τ_p . In b) we note that
 517 the oscillation appears mainly in the Southern Hemisphere, and is tightly connected to
 518 oscillations in the SH sea-ice extent. The Northern Hemisphere temperature is only slightly
 519 influenced by the oscillation, possibly through the atmosphere or because AMOC cou-
 520 ples it to the SH. AMOC data are not provided for this experiment, but temperature
 521 changes in the North Atlantic (not shown) indicate that AMOC is changing. The esti-
 522 mated parameters are listed in the figure, and shows also that we have allowed negative
 523 values of S_{osc1} and S_{osc2} . The physical interpretation of this is that the SH sea ice ac-
 524 tually decreases on average in extent, hence contributing to a warming on an otherwise
 525 cooling globe.

526 This oscillation seems to have a different physical origin than the oscillations/plateaus
 527 we observe in warming experiments. Similar changes in the SH were observed in the pi-
 528 Control experiment of this model (Ridley et al., 2022). In the piControl the deeper ocean
 529 has not yet reached an equilibrium state and the drifting temperatures eventually cause
 530 the water column in the Weddell and Ross seas to become unstable, and start to con-
 531 vect up warmer deeper ocean water that melts the sea ice. We suspect the oscillations
 532 in the abrupt-0p5xCO₂ experiment is a similar phenomenon, except that in this run the
 533 cooling of the atmosphere and ocean surface layer brings the ocean column in the south-
 534 ern oceans faster into an unstable state. The more the surface is cooling, the larger the
 535 area can become where this instability and melting of sea ice happens, which can explain
 536 the growing oscillation and overall reduced sea ice cover.

537 7.3 Multidecadal pauses in global temperature increase

538 In Fig. 7 it can be observed that the abrupt-4xCO₂ simulations for several models (e.g., GISS-
 539 E2.1-G, MRI-ESM2.0, SAM0-UNICON) exhibit a plateau in their global mean surface
 540 temperature evolution after the initial fast-paced increase. This happens typically be-
 541 tween years 30 and 70 and after year 70 the temperature starts increasing again. Av-
 542 eraging the temperature separately over northern and southern hemisphere (NH and SH,

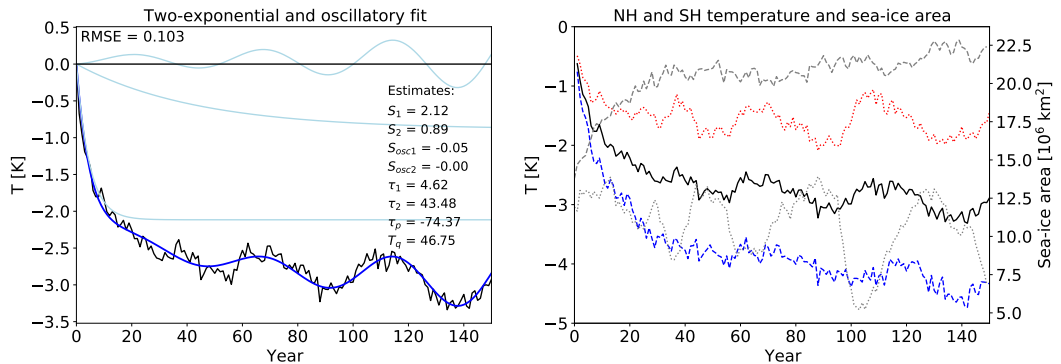


Figure 9. Results from HadGEM-GC31-LL abrupt-0p5xCO₂ r1i1p1f3, where allowing an unstable (growing) oscillation makes a good fit. a) The black curve is the global surface air temperature change relative to piControl, the thick blue curve is the fitted model consisting of two exponential components (slowly varying light blue curves) and one oscillatory pair (plotted together as the oscillating light blue curve). Note that to make the fit the signs were flipped, such that the listed parameters $S_1, S_2, S_{osc1}, S_{osc2}$ are consistent with a positive response. b) The global temperature response (black) split up in Northern Hemisphere (NH, dashed blue) temperature and Southern Hemisphere (SH, dotted red) temperature. On the right axis we have the sea-ice area, which is plotted for the SH (dotted gray) and NH (dashed gray).

respectively; see Fig. 10 for the example of GISS-E2.1-G) reveals that the plateau of the global mean temperature results from a plateauing or even decrease of the NH temperature while the SH temperature increases monotonically. More specifically, maps of time slices of surface warming make clear that it is the North Atlantic that cools in response to the CO₂-forcing (Fig. 10, left column). Models that do not exhibit the plateauing global mean temperature typically exhibit neither the plateauing in the NH nor the cooling (or lack of warming) in the North Atlantic (E3SM-1.0 shown as an example in Fig. 10, right column). Though there may be models where the North Atlantic cools/warms less, but not enough to cause a significant slowdown of global temperature increase.

The difference in North Atlantic temperatures between models with and without plateau is found to be concomitant with a difference in the development of AMOC and the development of Arctic sea ice (see Figure 10), consistent with earlier studies (Bellomo et al., 2021; Mitevski et al., 2021). Models with plateauing global mean temperature tend to simulate a stronger AMOC decline in response to the CO₂-forcing (e.g. GISS-E2-1-G and SAM0-UNICON) than do the models without plateau. Notably, the pre-industrial AMOC also tends to be stronger in models with plateau than in those without plateau. Furthermore, models with plateau retain more of their Arctic sea ice than models without plateau. The connection between a plateauing global temperature, weakening AMOC, and enhanced NH sea ice cover was also noted by Held et al. (2010) for the GFDL Climate Model version 2.1.

A stronger decline in AMOC is consistent with lower North Atlantic temperatures (Bellomo et al., 2021) and less sea ice melt (Yeager et al., 2015; Liu et al., 2020; Eiselt & Graversen, 2023). The AMOC constitutes a part of the poleward energy transport in the climate system that is necessary to balance the differential energy input from solar radiation. The AMOC accomplishes northward energy transport by transporting warm water from the Tropics into the Arctic increasing the ocean heat release there and thus warming the North Atlantic. A decline of the AMOC will hence lead to a cooling or at least a hampering of the warming in response to a CO₂-forcing. Growing sea ice in response to a cooling

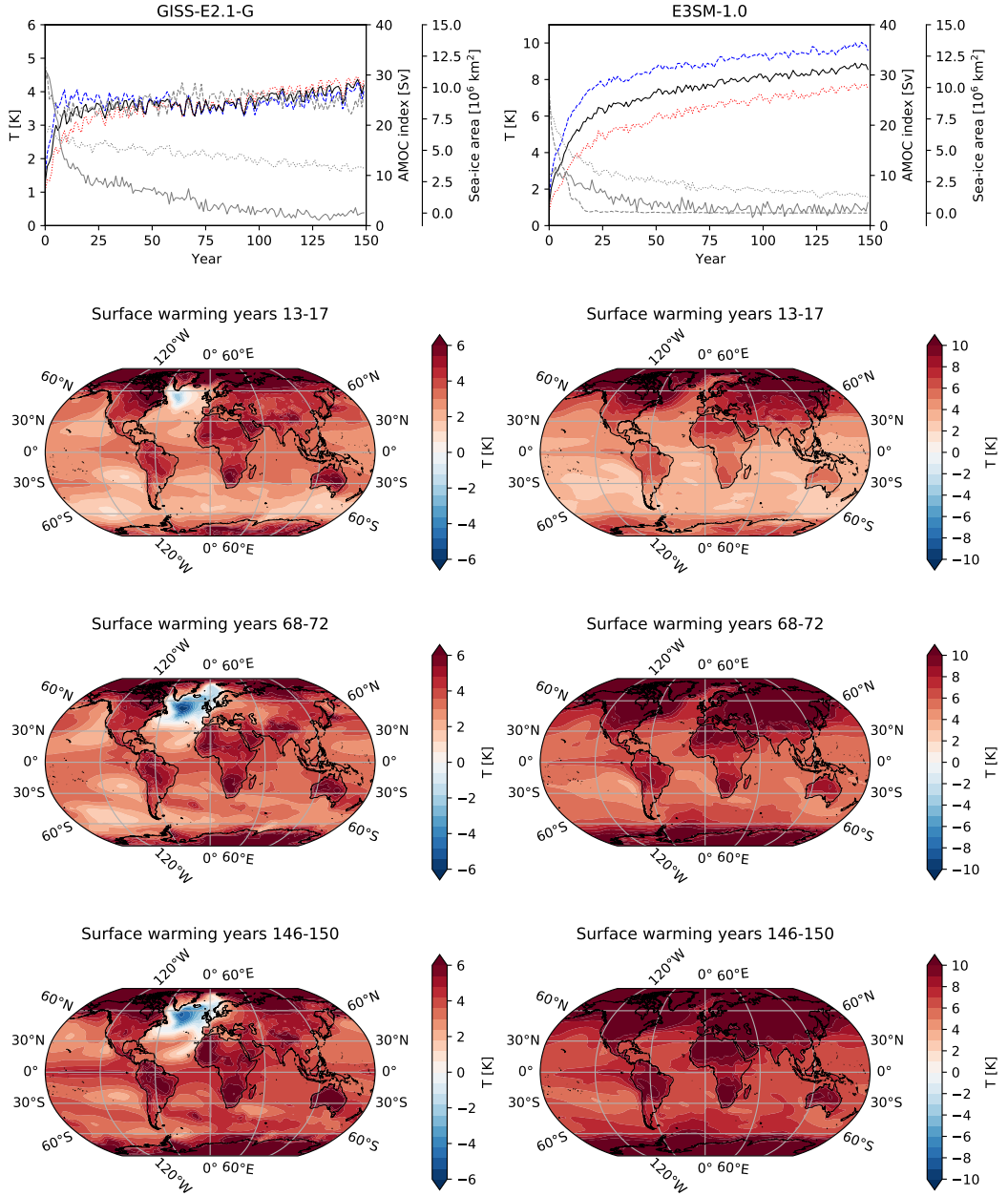


Figure 10. Example of models with and without plateaus in global temperature.

571 will contribute to keeping the temperature low for a while. Changes in sea ice has also
 572 been shown to affect AMOC (Sévellec et al., 2017; Liu et al., 2019; Madan et al., 2023).
 573 The growth of sea ice can therefore be an explanation for an eventual AMOC recovery,
 574 and finally lead to a decay of the oscillating component.

575 8 Discussion

576 Many earlier studies comparing different abrupt CO₂ experiments focus on experiments
 577 from single models, and are often mainly interested in the equilibrium response. Such
 578 studies find both decreasing and increasing climate sensitivities with stronger CO₂ forcing
 579 (see discussions in Meraner et al. (2013); Bloch-Johnson et al. (2021)), but the more
 580 comprehensive analysis by Bloch-Johnson et al. (2021) (including many of the same models
 581 as this paper) finds that climate sensitivity increases in most models.

582 Slab-ocean models are used in several studies (Colman & McAvaney, 2009; Meraner et
 583 al., 2013), and are useful tools for studying the temperature-dependence of atmospheric
 584 feedbacks. They are relatively cheap to run, and the pattern effect is somewhat suppressed
 585 in these models, partly because they go quicker to equilibrium and partly due to the lack
 586 of ocean dynamics that can change the pattern of the temperature response. This makes
 587 it easier to separate the nonlinear/temperature dependent feedbacks from the pattern
 588 effect, but ignores also possible permanent changes in feedbacks due to changes in the
 589 ocean circulation.

590 For a wide range of abrupt CO₂ increase experiments (1x to 8x), Mitevski et al. (2021)
 591 finds that the increase in effective climate sensitivity with increasing CO₂ is not mono-
 592 tonic in two fully coupled models (GISS-E2.1-G and CESM-LE), in contrast to the mono-
 593 tonic increase found in slab-ocean experiments (Meraner et al., 2013; Mitevski et al., 2021).
 594 The nonmonotonic increase is related to the decreasing temperatures in the North At-
 595 lantic and the weakening AMOC. For small enough abrupt CO₂ concentration increases
 596 (up to 2x and 3x CO₂ for GISS-E2.1-G and CESM-LE, respectively) the AMOC recov-
 597 ers after the initial decrease, while for higher concentrations it does not. For higher con-
 598 centrations, the North Atlantic cools less however, because of the increased warming from
 599 CO₂.

600 Manabe and Stouffer (1993, 1994) also focused on studying the thermohaline circulation
 601 in the Atlantic Ocean in different abrupt CO₂ experiments. In their 2x and 4x exper-
 602 iments they observe a weakening of the thermohaline circulation. The circulation recov-
 603 ered again for 2xCO₂, but remained weak for 4xCO₂. For 0.5xCO₂ Stouffer and Man-
 604 abe (2003) finds a weak and shallow thermohaline circulation in the Atlantic.

605 The collapse of AMOC above a certain CO₂ level is an example of how a change in the
 606 ocean circulation can cause a nonlinear global temperature response. A change in cir-
 607 culation changes the surface temperature pattern, which further modulates which atmo-
 608 spheric feedbacks are triggered. In the case of a permanent collapse of AMOC, the new
 609 pattern and associated feedbacks are also permanently changed. In general, any change
 610 in effectiveness of deeper ocean heat uptake can depend on state, and therefore result
 611 in a nonlinear response. A warming of the surface can lead to a more stratified ocean
 612 with reduced vertical mixing. To some extent, however, the reduced heat uptake can still
 613 be approximated as a linear function of the surface temperature increase. We have also
 614 demonstrated the opposite effect here, that a cooling of the surface can lead to a linear
 615 oscillating response, as a result of ocean-sea ice dynamics in the Southern Ocean.

616 Linear response models can take many forms. Examples of physically motivated mod-
 617 els are the upwelling-diffusion models (Hoffert et al., 1980) used in the First IPCC re-
 618 port, and the temperature component of the FaIR emulator (Millar et al., 2017; Smith
 619 et al., 2018; Leach et al., 2021) used in AR6 (P. Forster et al., 2021). They are power-
 620 ful tools for e.g. the IPCC reports since they can be used to quickly explore a wider range

of forcing scenarios than that simulated by coupled models. We suggest that a generalised box model is easier to interpret, test and generalise than box models using an efficacy factor, since temperature components and different feedback parameters are more directly associated with the pattern of surface temperature evolution, instead of being indirectly associated through an efficacy factor. We do not have to assume anything about the distribution of the boxes as long as we are interested in global quantities, but in order to better constrain the values of the different feedback parameters, the additional information about the pattern can be useful.

629 9 Conclusions

We find that linear response is overall a good assumption for global surface temperatures. However, good predictions with linear response models are crucially dependent on good forcing estimates. Distinguishing between forcing and response is a challenge, and the uncertainty of forcing estimates is the main limitation to determining if a model has a linear response or not.

Mitevski et al. (2022) and Geoffroy and Saint-Martin (2020) highlight the importance of taking into account the nonlogarithmic dependence of the forcing on the CO₂ concentration. This implies stronger forcing for each CO₂ doubling, also consistent with recent findings of (He et al., 2023). He et al. (2023) finds that the stratospheric temperature impacts CO₂ forcing, and that other forcing agents affecting the stratospheric temperature therefore can modulate the CO₂ forcing. Such nonlinear interaction between forcing agents should be studied in further detail, as this deviates from a linear framework. We hope also the effort initiated by RFMIP (Pincus et al., 2016) to better constrain forcing estimates will be continued for more models and experiments in the future.

For models with a plateau in the global temperature response to an abrupt increase in CO₂ stemming from a cooling of the North Atlantic, the cooling component (which can be modelled with an oscillatory part) can counteract the warming from the slow centennial-millennial scale component for a long time. For these models, a response model with a single exponential response can actually be sufficient for many short-term prediction purposes. In CESM104 abrupt2x a single exponential explains the majority of the first decades after abrupt doubling of CO₂, and for all 140 years with linearly increasing forcing.

Parameter estimation taking into account the possibility for centennial-scale oscillations is difficult for short time series, like the typical 150 year abrupt CO₂ experiments. We encourage more models to run longer abrupt CO₂ experiments, also for different levels of CO₂. Longer runs will help constrain linear response models better on the longer term, which can then further be used to quickly predict a wide range of other forcing scenarios. In particular, more and longer abrupt-2xCO₂ would be useful, since these are very likely to be within the range where a linear response is a good approximation. Linear responses estimated from abrupt-4xCO₂ are also quite good approximations, but there are some signs of nonlinear responses playing a role in these experiments (Fredriksen et al., 2023; Bloch-Johnson et al., 2021). CMIP6 abrupt-4xCO₂ warms on average 2.2 times abrupt-2xCO₂, and we estimate that about a factor 2 can be attributed to the forcing difference. The remaining 10% extra warming in abrupt-4xCO₂ is likely attributed to nonlinear responses, such as feedback changes (Bloch-Johnson et al., 2021).

664 References

- Andrews, T., Gregory, J. M., & Webb, M. J. (2015). The Dependence of Radiative Forcing and Feedback on Evolving Patterns of Surface Temperature Change in Climate Models. *Journal of Climate*, 28(4), 1630–1648. doi: 10.1175/JCLI-D-14-00545.1
- Andrews, T., Smith, C. J., Myhre, G., Forster, P. M., Chadwick, R., & Ackerley, D. (2021). Effective Radiative Forcing in a GCM With Fixed Surface Tempera-

- 671 tures. *Journal of Geophysical Research: Atmospheres*, 126, e2020JD033880.
672 doi: 10.1029/2020JD033880

673 Armour, K. C., Bitz, C. M., & Roe, G. H. (2013). Time-Varying Climate Sensitivity
674 from Regional Feedbacks. *Journal of Climate*, 26, 4518–4534. doi: 10.1175/
675 JCLI-D-12-00544.1

676 Bellomo, K., Angeloni, M., Corti, S., & von Hardenberg, J. (2021). Future cli-
677 mate change shaped by inter-model differences in Atlantic meridional over-
678 turning circulation response. *Nature Communications*, 12, 3659. doi:
679 10.1038/s41467-021-24015-w

680 Bloch-Johnson, J., Pierrehumbert, R. T., & Abbot, D. S. (2015). Feedback temper-
681 ature dependence determines the risk of high warming. *Geophysical Research
682 Letters*, 42(12), 4973–4980. doi: 10.1002/2015GL064240

683 Bloch-Johnson, J., Rugenstein, M., Stolpe, M. B., Rohrschneider, T., Zheng, Y., &
684 Gregory, J. M. (2021). Climate Sensitivity Increases Under Higher CO₂ Levels
685 Due to Feedback Temperature Dependence. *Geophysical Research Letters*, 48,
686 e2020GL089074. doi: 10.1029/2020GL089074

687 Caldeira, K., & Myhrvold, N. P. (2013). Projections of the pace of warming follow-
688 ing an abrupt increase in atmospheric carbon dioxide concentration. *Environ-
689 mental Research Letters*, 8(3), 034039. doi: 10.1088/1748-9326/8/3/034039

690 Colman, R., & McAvaney, B. (2009). Climate feedbacks under a very broad range of
691 forcing. *Geophysical Research Letters*, 36(1). doi: 10.1029/2008GL036268

692 Cummins, D. P., Stephenson, D. B., & Stott, P. A. (2020). Optimal Estimation
693 of Stochastic Energy Balance Model Parameters. *Journal of Climate*, 33(18),
694 7909–7926. doi: 10.1175/JCLI-D-19-0589.1

695 Edwards, C., & Penney, D. (2007). *Differential equations and boundary value prob-
696 lems: Computing and modelling (Fourth edition)*. Pearson.

697 Eiselt, K.-U., & Graversen, R. G. (2023). On the Control of Northern Hemispheric
698 Feedbacks by AMOC: Evidence from CMIP and Slab Ocean Modeling. *Journal
699 of Climate*, 36(19), 6777–6795. doi: 10.1175/JCLI-D-22-0884.1

700 Etminan, M., Myhre, G., Highwood, E. J., & Shine, K. P. (2016). Radiative forc-
701 ing of carbon dioxide, methane, and nitrous oxide: A significant revision of
702 the methane radiative forcing. *Geophysical Research Letters*, 43(24), 12,614–
703 12,623. doi: 10.1002/2016GL071930

704 Forster, P., Storelvmo, T., Armour, K., Collins, W., Dufresne, J.-L., Frame, D., ...
705 Zhang, H. (2021). The Earth's Energy Budget, Climate Feedbacks, and Cli-
706 mate Sensitivity [Book Section]. In V. Masson-Delmotte et al. (Eds.), *Climate
707 change 2021: The physical science basis. contribution of working group i to
708 the sixth assessment report of the intergovernmental panel on climate change*
709 (p. 923–1054). Cambridge, United Kingdom and New York, NY, USA: Cam-
710 bridge University Press. doi: 10.1017/9781009157896.009

711 Forster, P. M., Richardson, T., Maycock, A. C., Smith, C. J., Samset, B. H., Myhre,
712 G., ... Schulz, M. (2016). Recommendations for diagnosing effective radiative
713 forcing from climate models for CMIP6. *Journal of Geophysical Research:
714 Atmospheres*, 121(20), 12,460–12,475. doi: 10.1002/2016JD025320

715 Fredriksen, H.-B., Rugenstein, M., & Graversen, R. (2021). Estimating Radiative
716 Forcing With a Nonconstant Feedback Parameter and Linear Response. *Jour-
717 nal of Geophysical Research: Atmospheres*, 126(24), e2020JD034145. doi: 10.
718 1029/2020JD034145

719 Fredriksen, H.-B., & Rypdal, M. (2017). Long-range persistence in global surface
720 temperatures explained by linear multibox energy balance models. *Journal of
721 Climate*, 30, 7157–7168. doi: 10.1175/JCLI-D-16-0877.1

722 Fredriksen, H.-B., Smith, C. J., Modak, A., & Rugenstein, M. (2023). 21st Century
723 Scenario Forcing Increases More for CMIP6 Than CMIP5 Models. *Geophysical
724 Research Letters*, 50(6), e2023GL102916. doi: 10.1029/2023GL102916

725 Geoffroy, O., & Saint-Martin, D. (2020). Equilibrium- and Transient-State Depen-

- 726 dencies of Climate Sensitivity: Are They Important for Climate Projections?
 727 *Journal of Climate*, 33(5), 1863 – 1879. doi: 10.1175/JCLI-D-19-0248.1
- 728 Geoffroy, O., Saint-Martin, D., Bellon, G., Volodire, A., Olivié, D., & Tytéca, S.
 729 (2013). Transient Climate Response in a Two-Layer Energy-Balance Model.
 730 Part II: Representation of the Efficacy of Deep-Ocean Heat Uptake and Val-
 731 idation for CMIP5 AOGCMs. *Journal of Climate*, 26(6), 1859–1876. doi:
 732 10.1175/JCLI-D-12-00196.1
- 733 Geoffroy, O., Saint-Martin, D., Olivié, D. J. L., Volodire, A., Bellon, G., &
 734 Tytéca, S. (2013). Transient Climate Response in a Two-Layer Energy-
 735 Balance Model. Part I: Analytical Solution and Parameter Calibration Using
 736 CMIP5 AOGCM Experiments. *Journal of Climate*, 26, 1841–1857. doi:
 737 10.1175/JCLI-D-12-00195.1
- 738 Good, P., Andrews, T., Chadwick, R., Dufresne, J.-L., Gregory, J. M., Lowe, J. A.,
 739 ... Shiogama, H. (2016). nonlinMIP contribution to CMIP6: model inter-
 740 comparison project for non-linear mechanisms: physical basis, experimental
 741 design and analysis principles (v1.0). *Geoscientific Model Development*, 9(11),
 742 4019–4028. doi: 10.5194/gmd-9-4019-2016
- 743 Good, P., Gregory, J. M., & Lowe, J. A. (2011). A step-response simple climate
 744 model to reconstruct and interpret AOGCM projections. *Geophysical Research
 745 Letters*, 38, L01703. doi: 10.1029/2010GL045208
- 746 Good, P., Gregory, J. M., Lowe, J. A., & Andrews, T. (2013). Abrupt CO₂ ex-
 747 periments as tools for predicting and understanding CMIP5 representative
 748 concentration pathway projections. *Climate Dynamics*, 40(3), 1041–1053. doi:
 749 10.1007/s00382-012-1410-4
- 750 Gregory, J. M., Andrews, T., & Good, P. (2015). The inconstancy of the transient
 751 climate response parameter under increasing CO₂. *Philosophical Transactions
 752 of the Royal Society A: Mathematical, Physical and Engineering Sciences*, 373,
 753 20140417. doi: 10.1098/rsta.2014.0417
- 754 Gregory, J. M., Ingram, W. J., Palmer, M. A., Jones, G. S., Stott, P. A., Thorpe,
 755 R. B., ... Williams, K. D. (2004). A new method for diagnosing radiative
 756 forcing and climate sensitivity. *Geophysical Research Letters*, 31, L03205. doi:
 757 10.1029/2003GL018747
- 758 Hansen, J., Sato, M., Ruedy, R., Nazarenko, L., Lacis, A., Schmidt, G. A., ...
 759 Zhang, S. (2005). Efficacy of climate forcings. *Journal of Geophysical Re-
 760 search: Atmospheres*, 110(D18). doi: 10.1029/2005JD005776
- 761 Hasselmann, K., Sausen, R., Maier-Reimer, E., & Voss, R. (1993). On the cold start
 762 problem in transient simulations with coupled atmosphere-ocean models. *Cli-
 763 mate Dynamics*, 9(6), 53–61. doi: 10.1007/BF00210008
- 764 He, H., Kramer, R. J., Soden, B. J., & Jeevanjee, N. (2023). State dependence
 765 of CO₂ forcing and its implications for climate sensitivity. *Science*, 382(6674),
 766 1051–1056. doi: 10.1126/science.abq6872
- 767 Held, I., Winton, M., Takahashi, K., Delworth, T. L., Zeng, F., & Vallis, G. (2010).
 768 Probing the Fast and Slow Components of Global Warming by Returning
 769 Abruptly to Preindustrial Forcing. *Journal of Climate*, 23, 2418 – 2427. doi:
 770 10.1175/2009JCLI3466.1
- 771 Hoffert, M. I., Callegari, A. J., & Hsieh, C.-T. (1980). The role of deep sea heat
 772 storage in the secular response to climatic forcing. *Journal of Geophysical Re-
 773 search: Oceans*, 85, 6667-6679. doi: 10.1029/JC085iC11p06667
- 774 Jackson, L. S., Maycock, A. C., Andrews, T., Fredriksen, H.-B., Smith, C. J., &
 775 Forster, P. M. (2022). Errors in Simple Climate Model Emulations of Past and
 776 Future Global Temperature Change. *Geophysical Research Letters*, 49(15),
 777 e2022GL098808. doi: 10.1029/2022GL098808
- 778 Jiang, W., Gastineau, G., & Codron, F. (2023). Climate Response to Atlantic
 779 Meridional Energy Transport Variations. *Journal of Climate*, 36(16), 5399 –
 780 5416. doi: 10.1175/JCLI-D-22-0608.1

- Larson, E. J. L., & Portmann, R. W. (2016). A Temporal Kernel Method to Compute Effective Radiative Forcing in CMIP5 Transient Simulations. *Journal of Climate*, 29(4), 1497–1509. doi: 10.1175/JCLI-D-15-0577.1
- Leach, N. J., Jenkins, S., Nicholls, Z., Smith, C. J., Lynch, J., Cain, M., ... Allen, M. R. (2021). FaIRv2.0.0: a generalized impulse response model for climate uncertainty and future scenario exploration. *Geoscientific Model Development*, 14(5), 3007–3036. doi: 10.5194/gmd-14-3007-2021
- Lin, Y.-J., Hwang, Y.-T., Ceppi, P., & Gregory, J. M. (2019). Uncertainty in the Evolution of Climate Feedback Traced to the Strength of the Atlantic Meridional Overturning Circulation. *Geophysical Research Letters*, 46(21), 12331–12339. doi: 10.1029/2019GL083084
- Liu, W., Fedorov, A., & Sévellec, F. (2019). The Mechanisms of the Atlantic Meridional Overturning Circulation Slowdown Induced by Arctic Sea Ice Decline. *Journal of Climate*, 32(4), 977 – 996. doi: 10.1175/JCLI-D-18-0231.1
- Liu, W., Fedorov, A. V., Xie, S.-P., & Hu, S. (2020). Climate impacts of a weakened Atlantic Meridional Overturning Circulation in a warming climate. *Science Advances*, 6(26), eaaz4876. doi: 10.1126/sciadv.aaz4876
- Madan, G., Gjermundsen, A., Iversen, S. C., & LaCasce, J. H. (2023). The weakening AMOC under extreme climate change. *Climate Dynamics*. doi: 10.1007/s00382-023-06957-7
- Manabe, S., & Stouffer, R. J. (1993). Century-scale effects of increased atmospheric CO₂ on the ocean–atmosphere system. *Nature*, 364, 215 – 218. doi: 10.1038/364215a0
- Manabe, S., & Stouffer, R. J. (1994). Multiple-Century Response of a Coupled Ocean-Atmosphere Model to an Increase of Atmospheric Carbon Dioxide. *Journal of Climate*, 7(1). doi: 10.1175/1520-0442(1994)007<0005:MCROAC>2.0.CO;2
- Meraner, K., Mauritsen, T., & Voigt, A. (2013). Robust increase in equilibrium climate sensitivity under global warming. *Geophysical Research Letters*, 40(22), 5944–5948. doi: 10.1002/2013GL058118
- Millar, R. J., Nicholls, Z. R., Friedlingstein, P., & Allen, M. R. (2017). A modified impulse-response representation of the global near-surface air temperature and atmospheric concentration response to carbon dioxide emissions. *Atmospheric Chemistry and Physics*, 17(11), 7213–7228. doi: 10.5194/acp-17-7213-2017
- Mitevski, I., Orbe, C., Chemke, R., Nazarenko, L., & Polvani, L. M. (2021). Non-Monotonic Response of the Climate System to Abrupt CO₂ Forcing. *Geophysical Research Letters*, 48(6), e2020GL090861. doi: 10.1029/2020GL090861
- Mitevski, I., Polvani, L. M., & Orbe, C. (2022). Asymmetric Warming/Cooling Response to CO₂ Increase/Decrease Mainly Due To Non-Logarithmic Forcing, Not Feedbacks. *Geophysical Research Letters*, 49(5), e2021GL097133. doi: 10.1029/2021GL097133
- Pincus, R., Forster, P. M., & Stevens, B. (2016). The Radiative Forcing Model Intercomparison Project (RFMIP): experimental protocol for CMIP6. *Geoscientific Model Development*, 9(9), 3447–3460. doi: 10.5194/gmd-9-3447-2016
- Proistosescu, C., & Huybers, P. J. (2017). Slow climate mode reconciles historical and model-based estimates of climate sensitivity. *Sciences Advances*, 3, e1602821. doi: 10.1126/sciadv.1602821
- Richardson, T. B., Forster, P. M., Smith, C. J., Maycock, A. C., Wood, T., Andrews, T., ... Watson-Parris, D. (2019). Efficacy of Climate Forcings in PDRMIP Models. *Journal of Geophysical Research: Atmospheres*, 124(23), 12824–12844. doi: 10.1029/2019JD030581
- Ridley, J. K., Blockley, E. W., & Jones, G. S. (2022). A Change in Climate State During a Pre-Industrial Simulation of the CMIP6 Model HadGEM3 Driven by Deep Ocean Drift. *Geophysical Research Letters*, 49(6), e2021GL097171. doi: 10.1029/2021GL097171

- 836 Rohrschneider, T., Stevens, B., & Mauritsen, T. (2019). On simple representations
 837 of the climate response to external radiative forcing. *Climate Dynamics*, 53(5),
 838 3131–3145. doi: 10.1007/s00382-019-04686-4
- 839 Rugenstein, M., Bloch-Johnson, J., Abe-Ouchi, A., Andrews, T., Beyerle, U., Cao,
 840 L., ... Yang, S. (2019). LongRunMIP: Motivation and Design for a Large Col-
 841 lection of Millennial-Length AOGCM Simulations. *Bulletin of the American
 842 Meteorological Society*, 100(12), 2551-2570. doi: 10.1175/BAMS-D-19-0068.1
- 843 Smith, C. J., Forster, P. M., Allen, M., Leach, N., Millar, R. J., Passerello, G. A., &
 844 Regayre, L. A. (2018). FAIR v1.3: a simple emissions-based impulse response
 845 and carbon cycle model. *Geoscientific Model Development*, 11(6), 2273–2297.
 846 doi: 10.5194/gmd-11-2273-2018
- 847 Smith, C. J., Kramer, R. J., Myhre, G., Alterskjær, K., Collins, W., Sima, A.,
 848 ... Forster, P. M. (2020). Effective radiative forcing and adjustments in
 849 CMIP6 models. *Atmospheric Chemistry and Physics*, 20(16), 9591–9618. doi:
 850 10.5194/acp-20-9591-2020
- 851 Stevens, B., Sherwood, S. C., Bony, S., & Webb, M. J. (2016). Prospects for narrow-
 852 ing bounds on Earth's equilibrium climate sensitivity. *Earth's Future*, 4(11),
 853 512-522. doi: 10.1002/2016EF000376
- 854 Stouffer, R. J., & Manabe, S. (2003). Equilibrium response of thermohaline circu-
 855 lation to large changes in atmospheric CO₂ concentration. *Climate Dynamics*,
 856 20, 759 – 773. doi: 10.1007/s00382-002-0302-4
- 857 Sévellec, F., Fedorov, A. V., & Liu, W. (2017). Arctic sea-ice decline weakens the
 858 Atlantic Meridional Overturning Circulation. *Nature Climate Change*, 7, 604 –
 859 610. doi: 10.1038/nclimate3353
- 860 Tang, T., Shindell, D., Faluvegi, G., Myhre, G., Olivie, D., Voulgarakis, A., ...
 861 Smith, C. (2019). Comparison of Effective Radiative Forcing Calculations Us-
 862 ing Multiple Methods, Drivers, and Models. *Journal of Geophysical Research: Atmo-
 863 spheres*, 124(8), 4382-4394. doi: 10.1029/2018JD030188
- 864 Winton, M., Takahashi, K., & Held, I. M. (2010). Importance of Ocean Heat Uptake
 865 Efficacy to Transient Climate Change. *Journal of Climate*, 23(9), 2333-2344.
 866 doi: 10.1175/2009JCLI3139.1
- 867 Yeager, S. G., Karspeck, A. R., & Danabasoglu, G. (2015). Predicted slowdown
 868 in the rate of Atlantic sea ice loss. *Geophysical Research Letters*, 42, 10704 –
 869 10713. doi: 10.1002/2015GL065364
- 870 Zhou, C., Wang, M., Zelinka, M. D., Liu, Y., Dong, Y., & Armour, K. C.
 871 (2023). Explaining Forcing Efficacy With Pattern Effect and State De-
 872 pendence. *Geophysical Research Letters*, 50(3), e2022GL101700. doi:
 873 10.1029/2022GL101700

874 10 Open Research

875 Code is available in github (<https://github.com/Hegebf/Testing-Linear-Responses>),
 876 and will be deployed in zenodo to get a doi when the manuscript is accepted. The CMIP6
 877 data are available through ESGF (<https://aims2.llnl.gov/search/?project=CMIP6/>),
 878 and the processed version used here is deployed in [https://doi.org/10.5281/zenodo
 .7687534](https://doi.org/10.5281/zenodo.7687534). LongRunMIP data can be accessed through <https://www.longrunmip.org/>.

880 Acknowledgments

881 We thank Jeff Ridley for discussions that helped us understand the behaviour of the model
 882 HadGEM-GC31-LL. We would also like to thank everyone who contributed to produc-
 883 ing the LongRunMIP and CMIP6 model data used in this study. The work of author
 884 Hege-Beate Fredriksen was partly funded by the European Union as part of the EPOC
 885 project (Explaining and Predicting the Ocean Conveyor). Views and opinions expressed
 886 are however those of the author(s) only and do not necessarily reflect those of the Eu-
 887 ropean Union. Neither the European Union nor the granting authority can be held re-
 888 sponsible for them. The work of Kai-Uwe Eiselt was part of the project UiT - Climate

Initiative, Ice-ocean-atmosphere interactions in the Arctic - from the past to the future, funded by the Faculty of Science and Technology, UiT the Arctic University of Norway. Peter Good was supported by the Met Office Hadley Centre Climate Programme funded by DSIT.

Appendix A Solution of generalized box model

Here we will derive the solution of a generalized box model, based on theory from Edwards and Penney (2007).

The general box model is given by the linear system:

$$\frac{d\mathbf{T}(t)}{dt} = \mathbf{C}^{-1}\mathbf{K}\mathbf{T}(t) + \mathbf{C}^{-1}\mathbf{F}(t) \quad (\text{A1})$$

We consider first the homogeneous problem

$$\frac{d\mathbf{T}_h(t)}{dt} = \mathbf{A}\mathbf{T}_h(t)$$

where $\mathbf{A} = \mathbf{C}^{-1}\mathbf{K}$. We note that the matrix of possible solutions (the fundamental matrix) is:

$$\Phi(t) = [\mathbf{v}_1 e^{\gamma_1 t} \mid \mathbf{v}_2 e^{\gamma_2 t} \mid \dots \mid \mathbf{v}_n e^{\gamma_n t}].$$

where \mathbf{v}_n are the eigenvectors corresponding to the eigenvalues γ_n of the matrix \mathbf{A} . If we also set an initial condition $\mathbf{T}(0) = \mathbf{T}_0$, the homogeneous solution takes the form:

$$\mathbf{T}_h(t) = \Phi(t)\Phi(0)^{-1}\mathbf{T}_0 \quad (\text{A2})$$

An alternative notation when \mathbf{A} consists of constant coefficients is the matrix exponential $e^{\mathbf{A}t} = \Phi(t)\Phi(0)^{-1}$, since

$$\frac{d\Phi(t)\Phi(0)^{-1}}{dt} = \frac{de^{\mathbf{A}t}}{dt} = \mathbf{A}e^{\mathbf{A}t} = \mathbf{A}\Phi(t)\Phi(0)^{-1}.$$

We note that the elements of $e^{\mathbf{A}t}$ are a linear combination of elements of $\Phi(t)$.

Consider the case where we have a pair of complex conjugate eigenvalues, $\gamma_1 = \bar{\gamma}_2$, $\mathbf{v}_1 = \bar{\mathbf{v}}_2$. Let $\mathbf{v}_2 = \mathbf{a} + i\mathbf{b}$ and $\gamma_2 = p + iq$, such that

$$\begin{aligned} \mathbf{v}_2 e^{\gamma_2 t} &= (\mathbf{a} + i\mathbf{b})e^{(p+iq)t} \\ &= (\mathbf{a} + i\mathbf{b})e^{pt}(\cos qt + i \sin qt) \\ &= e^{pt}(\mathbf{a} \cos qt - \mathbf{b} \sin qt) + ie^{pt}(\mathbf{b} \cos qt + \mathbf{a} \sin qt) \end{aligned}$$

Then the pair of complex eigenvalue solutions can instead be given by the real and complex part of the expression above, such that:

$$\Phi(t) = [e^{pt}(\mathbf{a} \cos qt - \mathbf{b} \sin qt) \mid e^{pt}(\mathbf{b} \cos qt + \mathbf{a} \sin qt) \mid \mathbf{v}_3 e^{\gamma_3 t} \mid \dots \mid \mathbf{v}_n e^{\gamma_n t}].$$

The fundamental matrix of the homogeneous problem is also used to describe the particular solution to the original nonhomogeneous system:

$$\mathbf{T}_p(t) = e^{\mathbf{A}t} \int e^{-\mathbf{A}t} \mathbf{C}^{-1} \mathbf{F}(t) dt = \int e^{\mathbf{A}(t-s)} \mathbf{C}^{-1} \mathbf{F}(s) ds.$$

We assume that the forcing vector $\mathbf{F}(t)$ is a vector of constants \mathbf{w} multiplied by the global mean forcing $F(t)$. Further, we note that computing the matrix product $e^{\mathbf{A}(t-s)} \mathbf{C}^{-1}$ only results in extra constant factors to each entry of $e^{\mathbf{A}(t-s)}$, such that the resulting column vector obtained from $e^{\mathbf{A}(t-s)} \mathbf{C}^{-1} \mathbf{w}$ will therefore be a linear combination of the entries of $e^{\mathbf{A}(t-s)}$ (or $\Phi(t)$).

Finally, the global mean surface temperature $T(t)$ can be described as a linear combination (area-weighted average) of the components of the vector $\mathbf{T}_p(t) + \mathbf{T}_h(t)$,

$$T(t) = G^*(t)T_0 + \int_0^t G(t-s)F(s)ds \quad (\text{A3})$$

where

$$G(t) = e^{pt}(c_1 \cos qt - c_2 \sin qt) + e^{pt}(c_3 \cos qt + c_4 \sin qt) + \sum_{n=3}^K k_n e^{\gamma_n t} \quad (\text{A4})$$

$$= k_1 e^{pt} \cos qt + k_2 e^{pt} \sin qt + \sum_{n=3}^K k_n e^{\gamma_n t} \quad (\text{A5})$$

and $G^*(t)$ takes the same form as $G(t)$, but has different coefficients k_n . In case of more pairs of complex solutions, we can replace more pairs from $\sum_{n=3}^K k_n e^{\gamma_n t}$ by oscillatory solutions of the same form as $k_1 e^{pt} \cos qt + k_2 e^{pt} \sin qt$. For the system to be stable we must require the real part of each eigenvalue to be negative. And in the case of only real negative eigenvalues, all terms including cosines and sines are dropped from $G(t)$.

If we know the full history of the system instead of setting an initial value, the solution is given by

$$T(t) = \int_{-\infty}^t G(t-s)F(s)ds \quad (\text{A6})$$

Step-response

When studying the response to a unit-step forcing, we first decompose the response:

$$T(t) = \int_0^t G(t-s) \cdot 1 ds = \sum_{n=1}^K \int_0^t G_n(t-s)ds \quad (\text{A7})$$

where $G_1(t) = k_1 e^{pt} \cos qt$ and $G_2(t) = k_2 e^{pt} \sin qt$ describe the damped oscillatory responses, and $G_n(t) = k_n e^{\gamma_n t}$ describe responses associated with real negative eigenvalues. For the latter, we have the temperature responses

$$T_n(t) = \int_0^t G_n(t-s)ds = \int_0^t k_n e^{\gamma_n(t-s)}ds = S_n(1 - e^{\gamma_n t}) \quad (\text{A8})$$

where $S_n = -k_n/\gamma_n$. For $G_1(t)$, we find the step-response

$$\begin{aligned} T_1(t) &= \int_0^t G_1(t-s)ds = \int_0^t k_1 e^{p(t-s)} \cos q(t-s) ds \\ &= k_1 \left[\frac{e^{pt} (p \cos qt + q \sin qt) - p}{p^2 + q^2} \right] \\ &= S_{osc1} - S_{osc1} e^{pt} \cos qt + \frac{k_1 q}{p^2 + q^2} e^{pt} \sin qt \\ &= S_{osc1} \left[1 - e^{pt} \left(\cos qt - \frac{q}{p} \sin qt \right) \right] \end{aligned} \quad (\text{A9})$$

where $S_{osc1} = -\frac{k_1 p}{p^2 + q^2}$, and similarly for $G_2(t)$, we find

$$\begin{aligned} T_2(t) &= \int_0^t G_2(t-s)ds = \int_0^t k_2 e^{p(t-s)} \sin q(t-s) ds \\ &= k_2 \left[\frac{e^{pt} (p \sin qt - q \cos qt) + q}{p^2 + q^2} \right] \\ &= S_{osc2} - S_{osc2} e^{pt} \cos qt + \frac{k_2 p}{p^2 + q^2} e^{pt} \sin qt \\ &= S_{osc2} \left[1 - e^{pt} \left(\cos qt + \frac{p}{q} \sin qt \right) \right] \end{aligned} \quad (\text{A10})$$

where $S_{osc2} = \frac{k_2 q}{p^2 + q^2}$. The total step-response is therefore,

$$T(t) = S_{osc1} \left[1 - e^{pt} \left(\cos qt - \frac{q}{p} \sin qt \right) \right] + S_{osc2} \left[1 - e^{pt} \left(\cos qt + \frac{p}{q} \sin qt \right) \right] + \sum_{n=3}^K S_n (1 - e^{\gamma_n t}) \quad (\text{A11})$$

Finally, we note that if the forcing was stepped up to a different value than 1, this value will be a factor included in $S_{osc1}, S_{osc2}, \dots, S_n$.

Using step-response to derive other responses

If we have estimates of the parameters $S_{osc1}, S_{osc2}, \dots, S_n, p, q, \gamma_n$, we find that $k_1 = \frac{-S_{osc1}(p^2 + q^2)}{p}$, $k_2 = \frac{S_{osc2}(p^2 + q^2)}{q}$, $k_n = -S_n \gamma_n$, which we can plug into the expression for $G(t)$ and compute the response to other forcings.